7. Tumors

BOOK CHAPTER

Tumors

Nancy M. Major MD (chapter://search/Major%20Nancy M./%7B%22type%22:%22author%22%7D), Mark W. Anderson MD (chapter://search/Anderson%20Mark W./%7B%22type%22:%22author%22%7D), Clyde A. Helms MD (chapter://search/Helms%20Clyde A./%7B%22type%22:%22author%22%7D), Phoebe A. Kaplan MD (chapter://search/Kaplan%20Phoebe A./%7B%22type%22:%22author%22%7D) and Robert Dussault MD (chapter://search/Dussault%20Robert/%7B%22type%22:%22author%22%7D)
Musculoskeletal MRI (chapter://browse/book/3-s2.0-C20130189064), 7, 132-164

Magnetic resonance imaging (MRI) plays a central role in the work-up of a patient presenting with a suspected musculoskeletal tumor. MRI can confirm the presence of a lesion, allow for a specific diagnosis in some cases, define the extent of tumor spread, provide biopsy guidance, and assist in the evaluation of recurrent disease after therapy.

Therapeutic planning at the time of presentation is based primarily on the stage of the lesion. Local staging of a tumor depends on which anatomic structures and spaces (compartments) are involved, and this is best shown with MRI. Because an understanding of tumor staging is an important precursor to designing an optimal MRI protocol for evaluating these lesions, this chapter begins with a section briefly describing the principles of tumor staging. Despite

your understandable natural instinct to skip over this material, we strongly urge you to read it to understand better how to set up and interpret MRI studies for this important indication.

Staging of Musculoskeletal Tumors

Principles of Staging

The primary goal of the oncologic surgeon is to provide local control of disease by obtaining adequate tumor margins at the time of resection. If possible, this goal is achieved through a limb-sparing procedure; if the lesion is too advanced, an amputation or disarticulation is required. The decision to amputate or perform a limb-sparing procedure depends on many factors, including tumor size; relationship of the tumor to adjacent structures, such as nerves, vessels, and joints; and the overall stage of the tumor at the time of presentation.

Although there are different staging systems, they all are based on three components:

1. Grade of the tumor
2. Local extent of the tumor
3. Presence or absence of metastases

The Enneking staging system, which has been adopted by the Musculoskeletal Tumor Society, is outlined in Table 7.1 (t0010) .

Table 7.1

Sarcoma Staging

Stage	Grade (G)	Site (T)	Metastases (M)

Stage	Grade (G)	Site (T)	Metastases (M)
IA	Low (G1)	Intracompartmental (T1)	No (M0)
IB	Low (G1)	Extracompartmental (T2)	No (M0)
IIA	High (G2)	Intracompartmental (T1)	No (M0)
IIB	High (G2)	Extracompartmental (T2)	No (M0)
III	Any (G)	Any (T)	Yes (M1)
			Regional or distant

Grade

The grade of the tumor is a measure of its potential to metastasize. It is based primarily on histologic features and requires a preoperative biopsy. A sarcoma is classified as either low grade or high grade. Generally, a low-grade lesion is less biologically active and requires a relatively conservative surgical procedure. Conversely, a high-grade lesion usually necessitates a more radical procedure because of its more aggressive nature.

Local Extent

Factors related to the local extent of a tumor include its size and degree of involvement of adjacent tissues. Sarcomas tend to grow centrifugally along pathways of least resistance and are contained in part by a pseudocapsule as they extend into adjacent tissues. A malignant lesion may remain confined within the pseudocapsule (intracapsular); generally, however, malignant cells often extend beyond these capsular boundaries. If a lesion extends through its capsule but is still confined within a single anatomic compartment, it is considered extracapsular and intracompartmental. If the tumor extends into an adjacent compartment, it is classified as

extracompartmental. Extracompartmental spread may occur via direct tumor invasion of an adjacent compartment or by contamination resulting from fracture, hemorrhage, or an operative procedure such as an unplanned resection or poorly planned biopsy. Generally, lesions with more advanced local extension, including involvement of neurovascular structures or joints, require excision of more adjacent tissue than smaller tumors.

Metastases

The third component of the staging system is the presence or absence of nodal or distant metastases. Determination of metastases is usually accomplished with computed tomography (CT) and radionuclide bone scanning, but more recently, CT with positron emission tomography and whole-body MRI have been advocated as possible alternatives. Regional lymph node involvement is much less common with musculoskeletal sarcomas than are pulmonary metastases, but both are equally poor prognostic factors.

Principles of Imaging

Bone Tumors

MRI is the most sensitive imaging modality for detecting and delineating bone tumors, especially tumors involving the marrow cavity. The MRI appearance of most osseous lesions is very nonspecific, however, and conventional radiographs are essential for evaluating a primary bone tumor. Radiographs should be obtained early in the work-up of a symptomatic patient because they are inexpensive and provide the most specific information of any modality regarding the true nature of a lesion. The radiographic findings and degree of clinical suspicion dictate

further work-up. If an aggressive osseous lesion is identified on conventional radiographs, MRI is useful in the preoperative assessment of these patients because it is the best modality for local staging. If a bone lesion is clearly benign radiographically, MRI generally is unnecessary.

For a patient with normal radiographs, a radionuclide bone scan often is the next study obtained, as it can help localize the abnormality and allow for an appropriate field of view on MRI. Once a focal abnormality is detected, MRI is useful for further characterization. Even with a negative bone scan, MRI can detect radiographically occult intramedullary lesions and should be obtained in a patient with a known primary tumor and focal symptoms or laboratory abnormalities that suggest osseous metastases (Fig. 7.1 (f0010)). In this setting, a larger field of view is obtained with a marker placed on the skin at the site of pain in order for the region of interest to be appropriately evaluated.

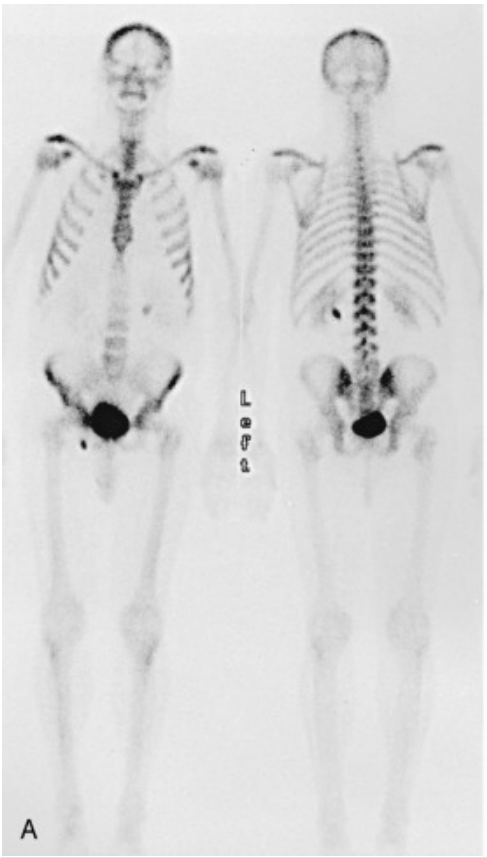

Fig. 7.1

Right iliac metastasis not detected on bone scan. **A** , Whole-body bone scan image. There is no scintigraphic evidence of metastasis in this 54-year-old man with a history of colon cancer and recent right hip pain. **B** , STIR coronal image of the pelvis. There is abnormal signal intensity within the right iliac bone (*arrow*) at the site of an osseous metastasis.

Soft Tissue Tumors

In a patient with a suspected soft tissue mass, conventional radiographs still should be obtained because they may reveal bone involvement or soft tissue calcifications that might be missed with MRI. In many cases, the MRI appearance of a soft tissue mass is so characteristic that a confident, specific diagnosis can be provided, obviating further work-up. Even if the MRI features do not allow a specific diagnosis to be made, MRI is still useful for staging these lesions.

Important MRI Features (Box 7.1 (b0010))

For osseous and soft tissue lesions, the crucial factors influencing resectability that should be addressed in the MRI report include intraosseous and extraosseous tumor extent and neurovascular, joint, and nodal involvement.

BOX 7.1

Checklist for Staging Musculoskeletal Tumor on MRI

- Intraosseous extent
- Extraosseous extent

- Neurovascular involvement
- Joint invasion
- Skip metastases in same bone
- Local adenopathy

Intraosseous Tumor Extent

Intraosseous tumor extent is best determined with T1-weighted (T1W) and short tau inversion recovery (STIR)/fat-saturated T2-weighted (T2W) imaging (Fig. 7.2 (f0015)); however, the intraosseous extent of tumor may be overestimated with STIR because it can be difficult to separate an intraosseous tumor from peritumoral edema on these images. MRI also is able to detect skip lesions (foci of tumor that are not contiguous with the primary lesion), which may be missed with scintigraphy.


A
B
C
D

Fig. 7.2

MRI evaluation of local extent of tumor. **A** , T1 sagittal image of the proximal tibia. A large tumor (plasmacytoma) is seen in the proximal tibia with intraosseous (*black arrows*) and extraosseous (*white arrow*) components. **B** , STIR sagittal image of the proximal tibia. The intraosseous and extraosseous components of the tumor are well shown. Note the associated edema within the adjacent musculature (*arrow*). **C** , STIR axial image of the proximal calf. The medial extraosseous tumor is well shown (*arrowhead*); however, the tumor is difficult to separate from adjacent muscle laterally (*arrow*). **D** , T1 axial image of the proximal calf. The lateral extraosseous component (*arrow*) is easier to delineate from adjacent edema and muscles. Note the normal fatty striations within the uninvolved skeletal muscle (*arrowheads*).

Extraosseous Tumor Extent

The extent of an extraosseous tumor is best evaluated with T2W or STIR imaging (see Fig. 7.2 (f0015)). Most tumors become hyperintense to fat on these sequences, and it may be difficult to separate tumor from adjacent soft tissue edema. MRI features of edema that help differentiate it from neoplasm include feathery margins, an absence of mass effect, and no distortion of muscle planes (see Fig. 7.2 (f0015)). Because a 5-cm “cuff” of normal tissue beyond the tumor margins usually is desired at surgery, exact measurements of the intraosseous and extraosseous components should be provided with reference to an osseous landmark (e.g., distance from the articular surface of the medial femoral condyle for a lesion involving the femoral shaft).

Neurovascular or Joint Involvement

Identification of neurovascular involvement is crucial (Fig. 7.3 (f0020)). Such involvement may preclude the possibility of a limb-sparing procedure because the functional status of a patient with a denervated limb after surgery may be worse than that achieved with an amputation. MRI is highly accurate in showing a lack of neurovascular involvement when a clear plane of normal tissue is shown between nerves or vessels and tumor. Gross tumor invasion usually is easily diagnosed, but if there is equivocal tumor involvement, this should be reported as such. The structures can be reassessed at the time of surgery. On a practical note, an anatomic atlas should be consulted in most cases to determine the expected position of pertinent nerves and vessels. Otherwise, neurovascular involvement might be overlooked if these structures are completely obliterated by a tumor.

Fig. 7.3

Neurovascular involvement. **A** , T1 sagittal image of the upper arm. A large tumor (osteosarcoma) involving the proximal humerus shows prominent extraosseous extension (*arrows*) and has resulted in a pathologic fracture. **B** , T1 axial image of the axilla. The tumor (*arrows*) is inseparable from and partially surrounds the circumflex humeral artery (H) and axillary nerve coursing through the quadrangular space (*arrowhead*). **C** , STIR sagittal image of the elbow (different patient than in **A** and **B**). A heterogeneous soft tissue mass (low-grade myxoid sarcoma) lies along the ventral surface of the distal humerus. **D** , T1 axial image of the elbow. The mass (M) displaces and compresses the radial neurovascular structures laterally. Although there appears to be preserved fat adjacent to the distorted radial nerve (*arrow*), tumor involvement is difficult to evaluate due to the degree of compression.

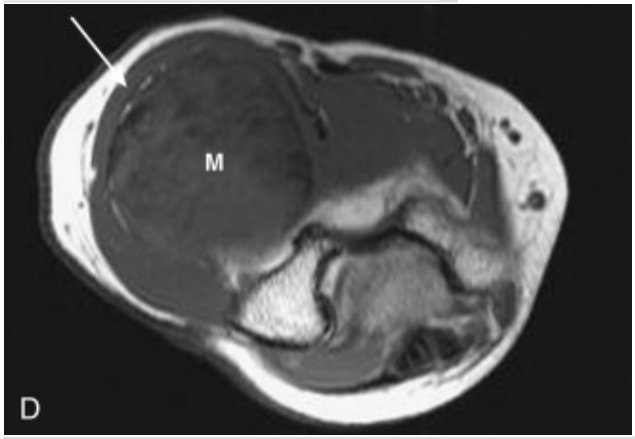

Because each joint is a distinct compartment, articular invasion changes the stage of a tumor and should be critically evaluated on every scan. MRI is very accurate for excluding joint involvement when the joint margins appear free of tumor, but is less accurate when the tumor is in close proximity to the joint. Close proximity results in a tendency to overcall joint invasion, which could result in an unnecessarily radical surgical procedure.

Nodes

Local and, when possible, regional lymph nodes should be assessed because nodal involvement carries the same poor prognosis as distant metastases in a patient with a musculoskeletal sarcoma.

Evaluation of Tumor After Therapy

Postchemotherapy

Survival of patients with musculoskeletal sarcomas has improved with the development of better adjuvant chemotherapeutic regimens. Assessing the degree of tumor response to chemotherapy is important for establishing the patient's prognosis and for planning further therapy. If viable tumor cells constitute less than 10% of a lesion after therapy, this indicates a good response (a "responder"), whereas more than 10% represents a poor response (a "nonresponder"). Currently, this response is determined after resection of the tumor, but several series have evaluated the use of MRI in this setting with conflicting results.

Changes in tumor size, signal intensity, or adjacent edema on conventional sequences are not sufficiently predictive to separate responders from nonresponders. Similarly, because tumor and non-neoplastic reactive tissue enhances on standard, postgadolinium T1W images, this technique is also unreliable for this purpose. Dynamic enhancement patterns on gadolinium-enhanced, rapid gradient echo–T1W sequences have shown a high degree of correlation with response or nonresponse because the residual tumor enhances more quickly than the reactive tissue does. We do not use these methods, however, because they are time consuming, technically challenging, and still not reliable enough to replace biopsy and histology.

Postsurgery and Postradiation

MRI is valuable for detecting tumor recurrence after surgical or radiation therapy, primarily because of its superb soft tissue contrast. MRI is sometimes too sensitive in this regard, as

postsurgical and postradiation changes in tissues can produce signal intensity that may be mistaken for neoplasm. Careful analysis of T1W, T2W, and STIR images, combined with an understanding of a few basic principles, can markedly improve the diagnostic accuracy of MRI in this setting. Postcontrast imaging may also be beneficial in certain cases, as described subsequently.

A lack of increased signal intensity on T2W or STIR images is a strong predictor of nonrecurrence, as a recurrent tumor usually shows high signal intensity on these images. There are other non-neoplastic causes of increased signal intensity in these patients, however, which can mimic a tumor, including radiation-induced edema and postoperative fluid collections such as hematoma, seroma, or abscess. Certain features help to separate these entities.

Surgery and radiation therapy often result in edema or hemorrhage within tissues, but the absence of a discrete mass is strong evidence against tumor recurrence. This can be evaluated on T1W images by looking for loss of the normal fatty marbling within muscle or distortion of the intermuscular fascial planes. The presence of normal skeletal muscle architecture in these regions on T1W images (normal “texture sign”) is highly predictive of nonrecurrence despite the presence of increased signal intensity on T2W images or enhancement after gadolinium administration (Fig. 7.4 (f0025)).

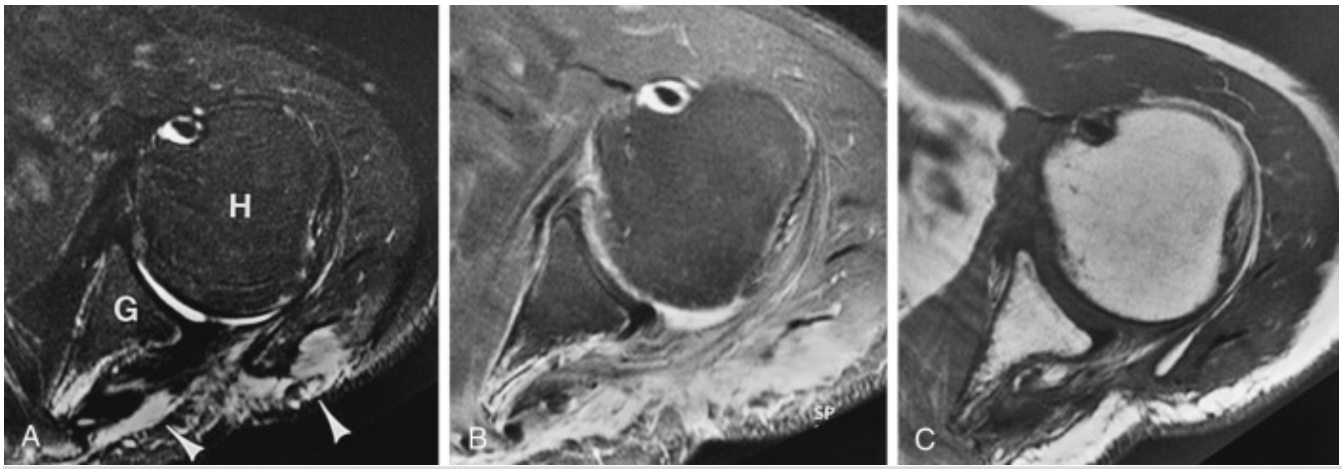

Fig. 7.4

Postsurgical changes. **A** , STIR axial image of the left shoulder. There is high signal intensity infiltrating the posterior soft tissues (*arrowheads*) in this patient, who had undergone prior sarcoma resection in this region. G, glenoid; H, humeral head. **B** , T1 axial image with fat saturation of the left shoulder after IV gadolinium administration. There is diffuse enhancement within the posterior soft tissues. **C** , T1 axial image of the left shoulder. There is no evidence of focal mass effect or distortion of muscle architecture in the areas of abnormal signal and enhancement, indicating that these findings do not represent tumor recurrence.

If a mass is discovered, administration of intravenous (IV) gadolinium may be helpful for further characterization. A postoperative lymphocele, seroma, or abscess appears as a high signal intensity mass on T2W images but does not show internal enhancement on postgadolinium T1W images (Fig. 7.5 (f0030)). If an enhancing mass is identified, biopsy is indicated because recurrent tumor is likely (Fig. 7.6 (f0035)); however, post-therapy granulation tissue also can enhance and produce an identical appearance.

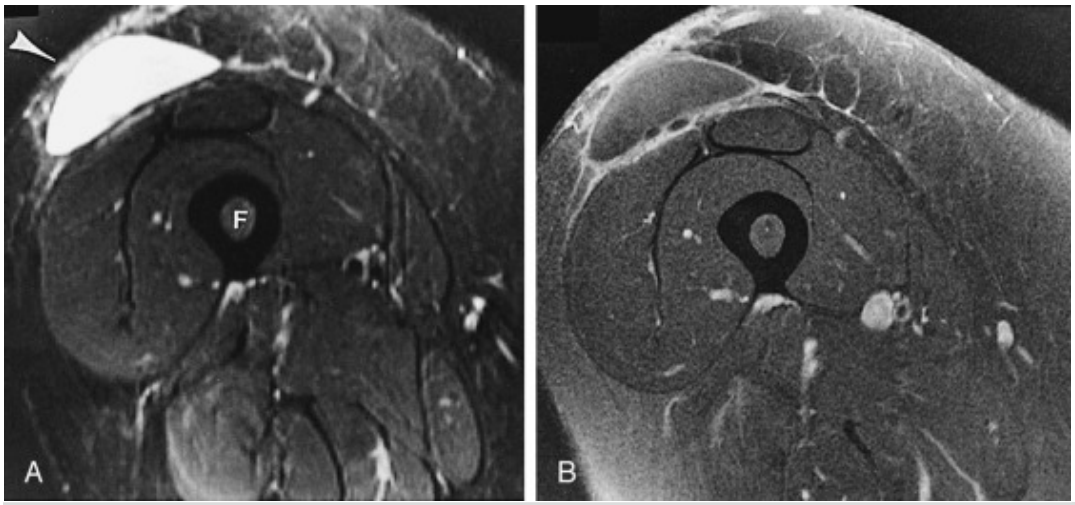

Fig. 7.5

Postoperative seroma. **A** , STIR axial image of the proximal right thigh. There is a well-marginated, lenticular-shaped mass (*arrowhead*) showing homogeneous high signal intensity within the subcutaneous fat at the site of prior sarcoma resection. *F,* Femur. **B** , T1 axial image with fat saturation of the proximal right thigh after the administration of IV gadolinium. There is enhancement of the periphery of the mass without central enhancement, confirming that this represents a postoperative fluid collection.

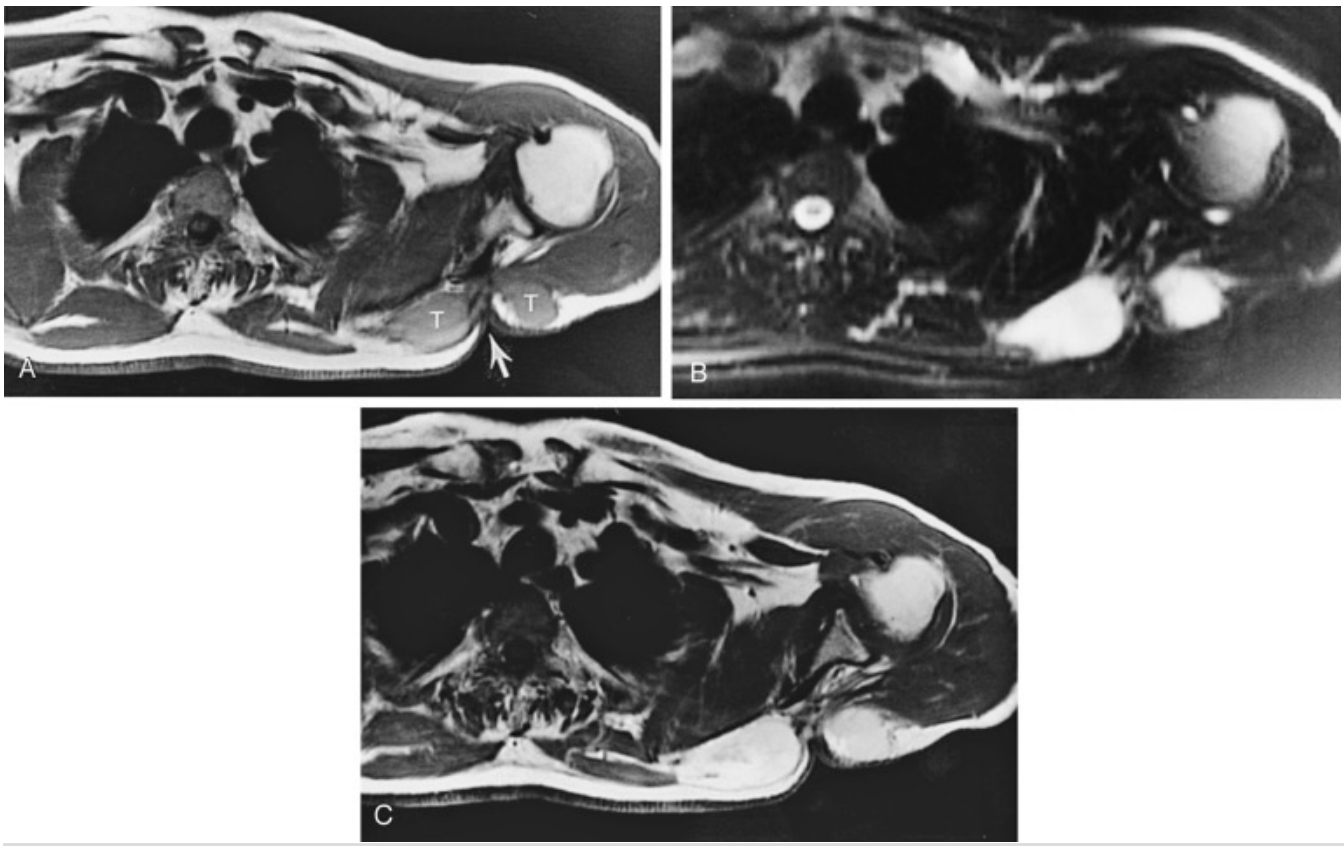

Fig. 7.6

Recurrent tumor. **A** , T1 axial image of the left chest. There is a scar (*arrow*) and postoperative deformity at the site of prior leiomyosarcoma resection. Additionally, there are two subcutaneous nodules at the operative site (T) showing intermediate signal intensity. **B** , STIR axial image of the left chest. Both masses show diffusely increased signal intensity. **C** , Axial T1 image of the left chest after IV administration of gadolinium. Both masses exhibit diffuse enhancement and were shown to represent recurrent sarcoma at subsequent surgery.

How to Image Tumors

Based on these principles, an imaging protocol can be designed that provides the information needed for accurate staging or post-therapy follow-up.

- *Coils and patient position:* In most cases, the patient is scanned in a supine position. Rarely, a prone position may allow for improved comfort and less motion artifact (e.g., when scanning the sternum). We typically begin with a sequence using the body coil and a large field of view to ensure that all portions of the primary tumor are identified. This is important for surgical planning, identifying skip or metastatic lesions, and designing additional sequences. When the extent of the tumor has been documented, higher-resolution images should be obtained, using a surface coil whenever possible. This provides for optimal assessment of tumor margins and involvement of neurovascular or joint structures.

• *Image orientation:* The initial large field-of-view sequence should be performed in a coronal or sagittal plane to best display the entire length of the lesion. Axial images are obtained with a smaller field of view to delineate tumor margins and neurovascular or articular involvement. These should be supplemented with additional longitudinal images to produce images that are tangential, rather than en face, to the lesion. Sagittal images are most helpful for a mass involving the anterior or posterior tissues of an extremity, whereas coronal images are used for lesions that are primarily medial or lateral in location.

• *Pulse sequences and regions of interest:* For this chapter, when STIR imaging is mentioned, T2W imaging with fat saturation could also be used. Historically, we have preferred the STIR technique because of its more consistent homogeneous fat saturation, but as MRI technology has progressed, this has become less of a factor.

• A skin marker should be placed over the suspected mass to confirm that the tissues of interest have been covered. In a postoperative patient, the entire length of the scar should be imaged. STIR imaging is most helpful for the initial large field-of-view sequence because it is very sensitive to neoplastic tissue and associated edema or hemorrhage. It is also superb for detecting any skip or metastatic lesions. It may be difficult to differentiate tumor from edema in the medullary canal on STIR images alone, and an additional body coil coronal or sagittal T1W sequence is a useful adjunct because of the sharp contrast between tumor and fat on this sequence. T1W images are also

useful for defining anatomy and detecting high signal fat or hemorrhage within a lesion. Axial T1W and STIR images are obtained, followed by T1 and fast spin echo–T2W or STIR images in a longitudinal plane, using a surface coil, if possible, so that tumor margins and involvement of adjacent structures are better resolved. A word of caution regarding fast spin echo–T2W sequences: the relatively bright signal intensity of fat on these images is similar to that of most pathologic processes, and this may mask an intramedullary lesion. Fat saturation should be routinely used with this sequence to improve lesion detection. Gradient echo sequences are not a part of our routine tumor protocol, although these can be used for evaluating flow within a lesion or adjacent vessels. This technique is also useful for detecting the presence of hemosiderin within a hematoma or an area of pigmented villonodular synovitis.

• *Contrast enhancement:* We do not administer IV gadolinium as part of our standard tumor protocol, but do use it when attempting to differentiate cystic from cystic-appearing solid lesions. When doing so, if fat saturation is to be used on postcontrast T1W images, it is imperative to perform a precontrast T1W fat-saturated series in the same plane to avoid the potential pitfall of “pseudoenhancement” resulting from changing two variables at once (contrast and fat saturation) (Fig. 7.7 (f0040))

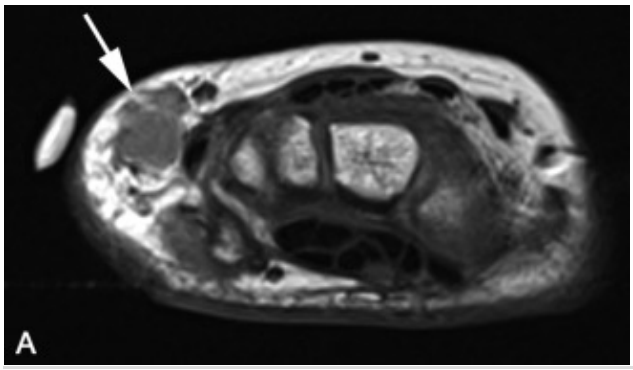

Fig. 7.7

Pseudoenhancement. **A,** T1 axial right wrist. A rounded mass isointense to muscle (*arrow)* is present within the subcutaneous tissues of the right wrist just deep to a skin marker. **B,** STIR axial. The mass demonstrates diffusely increased signal with a few internal septae and low signal intensity nodules. **C,** T1 axial with fat saturation before contrast administration. Note the relatively increased signal within the mass compared with the T1W image without fat saturation **(A).** This "pseudoenhancement" results from changes in how the soft tissue contrast is displayed when the signal from fat is suppressed. **D,** T1W axial with fat saturation after contrast administration. No enhancement is identified when compared with the precontrast fat-saturated T1W image **(C)** ; however, when compared to the T1W image without fat suppression **(A)** the mass appears to "enhance."

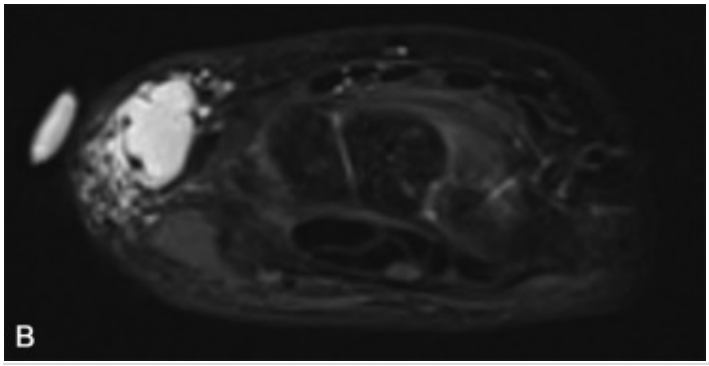

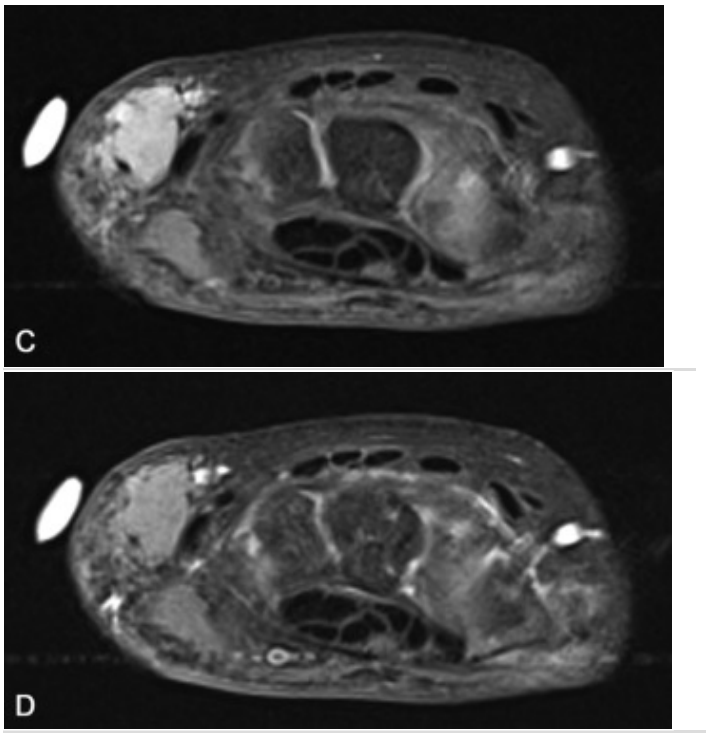

After surgical or radiation therapy, we use T1W and STIR sequences to image the area of interest and postgadolinium imaging to evaluate for any enhancing masses in the treatment area.

Approach to Image Interpretation

General Principles

Many benign lesions generally show smooth margins, homogeneous signal intensity, and a lack of involvement of neurovascular structures. Conversely, malignant masses tend to display heterogeneous signal, irregular margins, associated edema, and invasion of neurovascular or osseous structures.

However, there is a large amount of overlap in the appearances of benign and malignant lesions using these characteristics, and it can be dangerous to attempt to determine conclusively whether a mass is benign or malignant based solely on its MRI appearance (Fig. 7.8 (f0045)). Most lesions need to be classified as standard; T1W imaging after contrast administration has not been helpful in

differentiating benign from malignant lesions, although gadolinium-enhanced imaging using rapid T1W gradient echo sequences can provide some information regarding the malignant potential of a tumor based on the rate of enhancement. Benign tumors tend to enhance more slowly than malignant lesions, but in a given patient, we prefer to perform a biopsy of the lesion, rather than rely on statistical probability, because of the significant overlap between benign and malignant lesions.

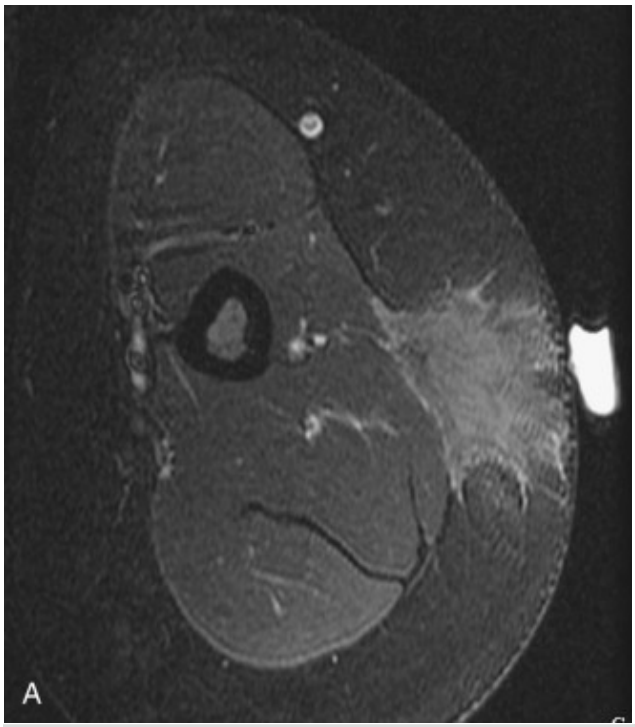

Fig. 7.8

Indeterminate soft tissue masses. **A** , STIR axial image of the upper arm. An ill-defined mass within the lateral subcutaneous tissues shows very irregular margins and superficial invasion of the underlying musculature. **B** , T1 fat-saturated axial image of the upper arm after gadolinium administration. The mass shows intense, diffuse enhancement. Biopsy revealed this to be a focus of benign, inflammatory tissue containing non-necrosing granulomatous changes. **C** , STIR axial image of the thigh (different patient than in **A** and **B**). An infiltrative mass in the subcutaneous tissues displays a similar MRI appearance to the lesion in **A** and **B** with irregular margins and superficial involvement of the underlying musculature. **D** , T1 fat-saturated axial image of the thigh after gadolinium administration. Diffuse enhancement is seen throughout the mass, which was found to be follicular lymphoma on biopsy.

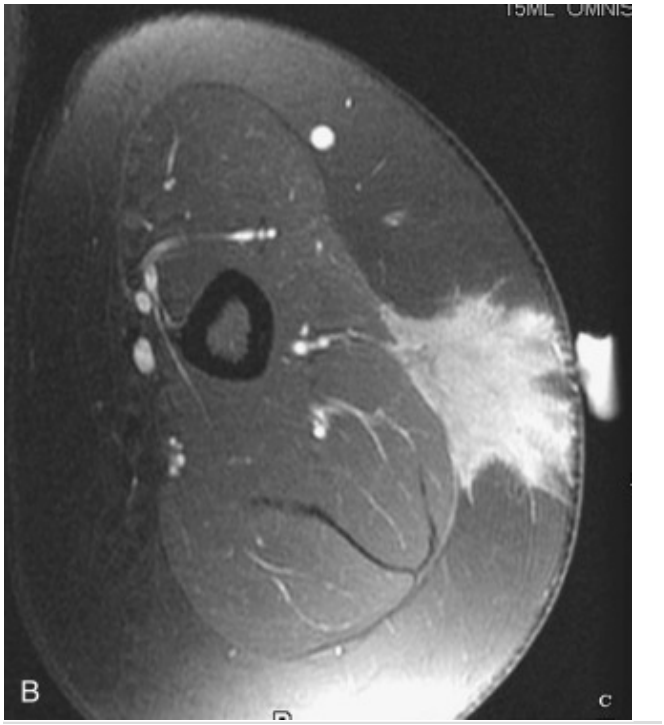

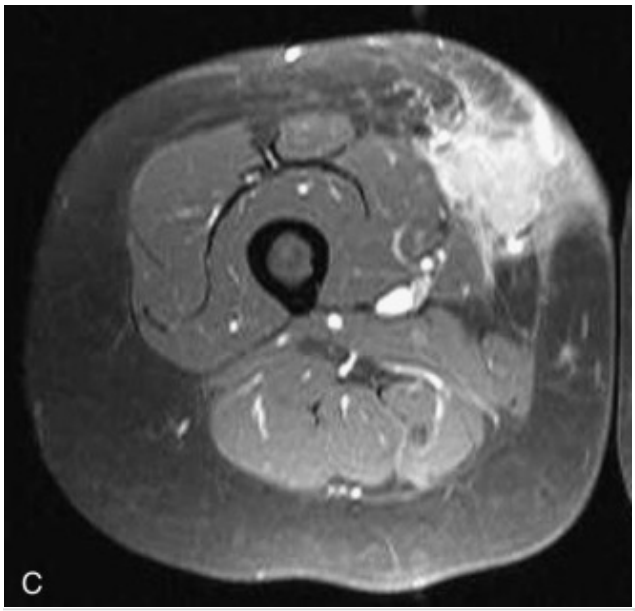

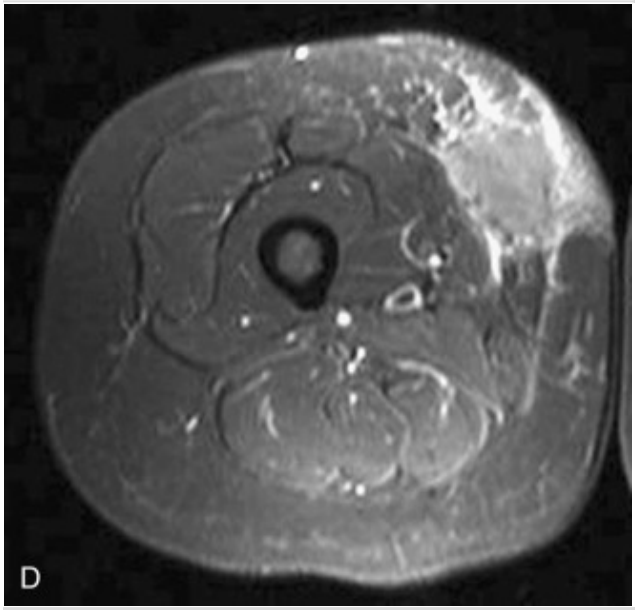

Bone Lesions

A reasonable differential diagnosis can be developed for most osseous lesions using the patient's age and the location of the lesion (within the skeleton and within the particular bone) and its radiographic appearance. For most bone tumors, MRI is used for staging, rather than for arriving at a specific diagnosis, because the true nature and aggressiveness of a lesion are determined much more accurately with conventional radiographs. Consequently, recent radiographs should always be viewed in conjunction with MR images; this is also important because some benign osseous

lesions display a very aggressive, potentially misleading appearance on MRI. These include osteoid osteoma, chondroblastoma, osteoblastoma, eosinophilic granuloma, and stress fracture (Fig. 7.9 (f0050)). The edema associated with these lesions often results in extensive signal abnormality in the medullary cavity and adjacent soft tissues, mimicking more aggressive lesions, such as osteomyelitis or malignant tumor.

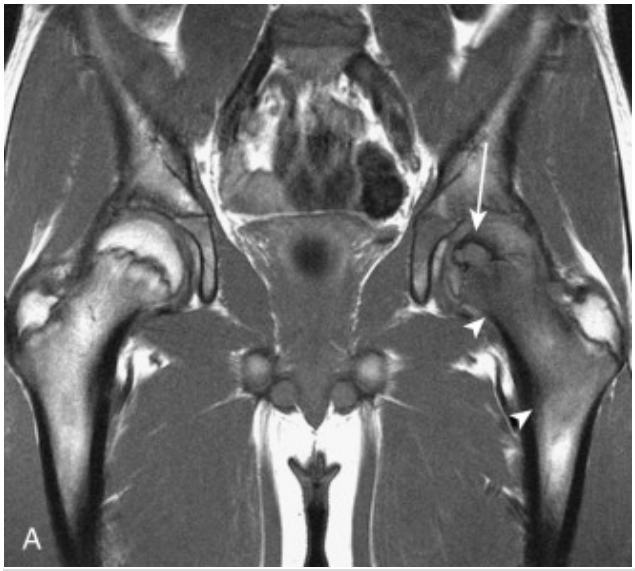

Fig. 7.9

Aggressive-appearing benign lesion. **A** , T1 coronal image of the pelvis. A focal lesion (*arrow*) is present within the proximal femoral epiphysis in this child who presented with hip pain. Note also the ill-defined, low signal intensity edema throughout the femoral neck (*arrowheads*). **B** , STIR coronal image of the pelvis. The mass is hyperintense, and associated marrow edema is shown throughout the femoral neck and in the medial portion of the acetabulum. Biopsy revealed Langerhans cell histiocytosis.

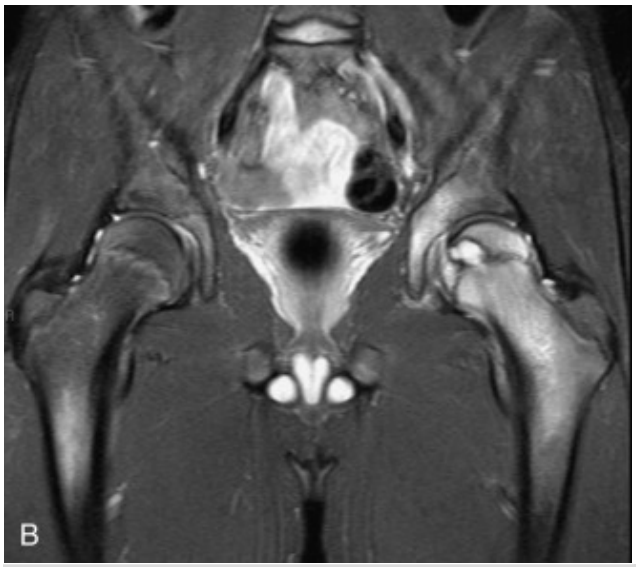

An osteoid osteoma is a cortically based lesion. The key to its diagnosis is to show a focal tumor nidus within the area of cortical/periosteal reaction. The tumor nidus typically displays low to intermediate signal intensity on T1W images, low or high signal on T2W images, and a variable degree of enhancement after gadolinium administration. There is usually a significant amount of surrounding marrow and soft tissue edema that can obscure the nidus and lead to an erroneous diagnosis (Fig. 7.10 (f0055)). In many cases, the nidus is more readily identified with CT.

Fig. 7.10

Marrow edema related to an osteoid osteoma. **A** , STIR coronal image of the pelvis. There is a geographic area of increased signal intensity within the left femoral neck (*arrowhead*), along with a moderate-sized left hip effusion. **B** , T2* (gradient echo) axial image of the proximal left femur. The tumor nidus is seen along the anterior left femoral neck as a small subcortical focus of increased signal intensity (*open arrow*).

Chondroblastoma should be suspected when a lesion is found in a skeletally immature patient with its epicenter in the epiphysis. Striking signal abnormality, corresponding to edema, often extends into the adjacent medullary cavity and may even extend to the metaphysis as well as overlying soft tissues.

In the case of a stress fracture, the presence of a linear fracture line within an area of marrow edema or cortical bone is diagnostic. In the absence of a fracture line, follow-up radiographs obtained 2 to

3 weeks later may be diagnostic. Biopsy should be avoided because the immature osteoid related to the healing process may be mistaken for malignancy at histology.

Differential Features

Although conventional radiographs provide the most specific information regarding the true nature of a bone tumor, some MRI features can help limit the differential diagnosis.

Increased Signal: T1W Images (Box 7.2 (b0015))

Intraosseous Lipoma

Intraosseous lipomas most commonly occur in the calcaneus, proximal femur, and humerus. They sometimes are difficult to differentiate from other lytic lesions on conventional radiographs but are easily recognized on MR images because of their predominant fat signal on all sequences. An intraosseous lipoma also may contain areas of increased or decreased signal intensity on T2W images, reflecting cystic degeneration or calcification (Fig. 7.11 (f0060)).

BOX 7.2

Bone Lesions Containing High Signal on T1W Images

- Intraosseous lipoma
- Hemangioma
- Bone infarct
- Paget's disease

Fig. 7.11

High signal intensity, T1: intraosseous lipoma affecting the femur. **A** , Frontal radiograph of the right hip. A mixed lytic and sclerotic lesion is seen in the proximal right femur. **B** , T1 coronal image of the pelvis. Extensive high signal intensity fat is seen within the lesion (*arrowheads*), along with a focus of low signal intensity centrally (*arrow*) corresponding to the dense calcification shown on the radiograph.

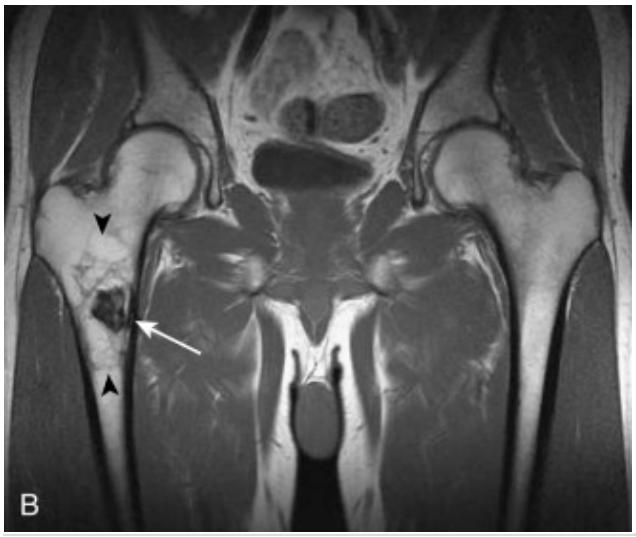

Intraosseous Hemangioma

Intraosseous hemangiomas are extremely common in the spine. Simple hemangiomas display increased signal intensity on T2W images but are differentiated from other lesions by high signal intensity on T1W images caused by their fat content (Fig. 7.12 (f0065)). Alternatively, hypervascular (aggressive) intraosseous hemangiomas typically do not contain fat and are indistinguishable from other tumors.

Fig. 7.12

High signal intensity, T1: intraosseous hemangioma. **A,** T2 sagittal image of the lumbar spine. A large, high signal intensity lesion is present within the L5 vertebra. **B,** T1 sagittal image of the lumbar spine. Extensive high signal intensity within the lesion indicates abundant fat consistent with a vertebral hemangioma.

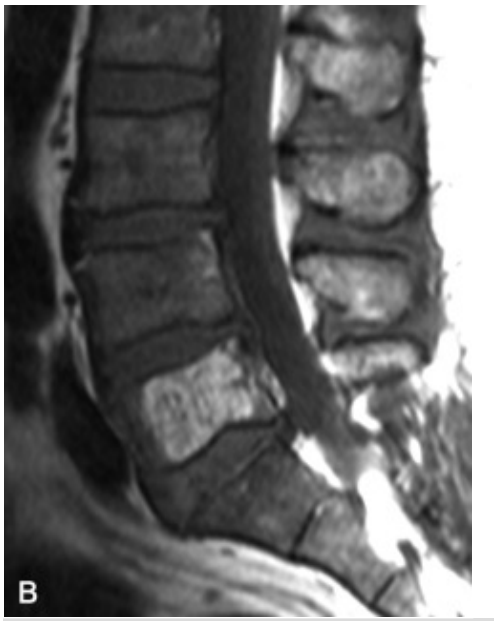

Medullary Bone Infarct

A medullary bone infarct is a geographic lesion with a serpentine, low signal intensity margin on T1W and T2W MR images. These usually contain centrally interspersed fat with foci of mixed signal intensity, corresponding to areas of fibrosis, calcification, or edema (Fig. 7.13 (f0070)).

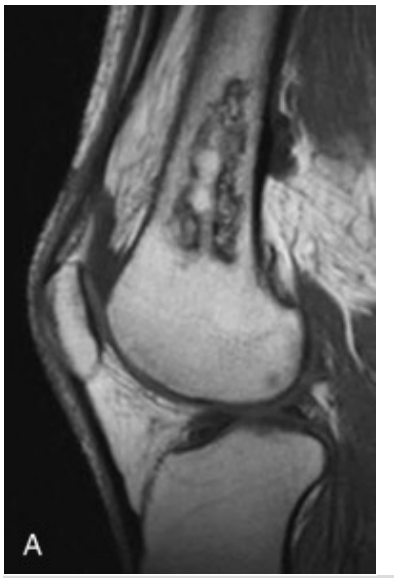

Fig. 7.13

High signal intensity, T1: medullary bone infarcts. **A** , T1 sagittal image of the knee. An irregular, geographic area of abnormal signal intensity within the medullary cavity of the distal femoral shaft is compatible with a medullary infarct. Note the low signal intensity serpentine margins and the extensive fat signal intensity within the lesion. **B** , T1 sagittal image of the ankle (different patient than in **A**). Similar lesions are seen within multiple bones of the ankle and hindfoot in this patient who had a long history of steroid therapy. **C** , STIR sagittal image of the ankle. High and low signal intensity bands are seen along the margins of the infarcts (“double-line sign”). Note also the suppressed fat within the central portions of the lesions.

Paget's Disease

The MRI appearance of Paget's disease varies. Areas of fat are commonly found within involved areas, but more heterogeneous signal intensity, corresponding to hypervascular marrow, may be seen in the active stage of the disease (Fig. 7.14 (f0075)). Other findings, such as cortical thickening, bone enlargement, and prominent, coarse trabeculae, are often better shown on conventional radiographs.

Fig. 7.14

High signal intensity, T1: Paget's disease. **A** , Lateral radiograph of the lumbar spine. Classic features of Paget's disease are present within the L4 vertebra (*arrowhead*), including increased sclerosis, thickening of the end plates and trabeculae, and mild overall enlargement of the vertebra relative to adjacent vertebral bodies. **B** , T1 sagittal image of the lumbar spine. There is prominent fat signal intensity within the vertebral body, especially in its posterior portion.

Decreased Signal: T2W Images (Box 7.3 (b0020))

Sclerosis/Calcification/Matrix

The presence of extremely low signal intensity within an osseous lesion on T2W images suggests sclerotic bone, calcification, or osteoid/chondroid tumor matrix. These are better characterized with conventional radiographs or CT (Fig. 7.15 (f0080)).

BOX 7.3

Bone Lesions Containing Low Signal on T2W Images

- Sclerosis/calcification/matrix
- Some fibrous lesions
- Primary lymphoma of bone

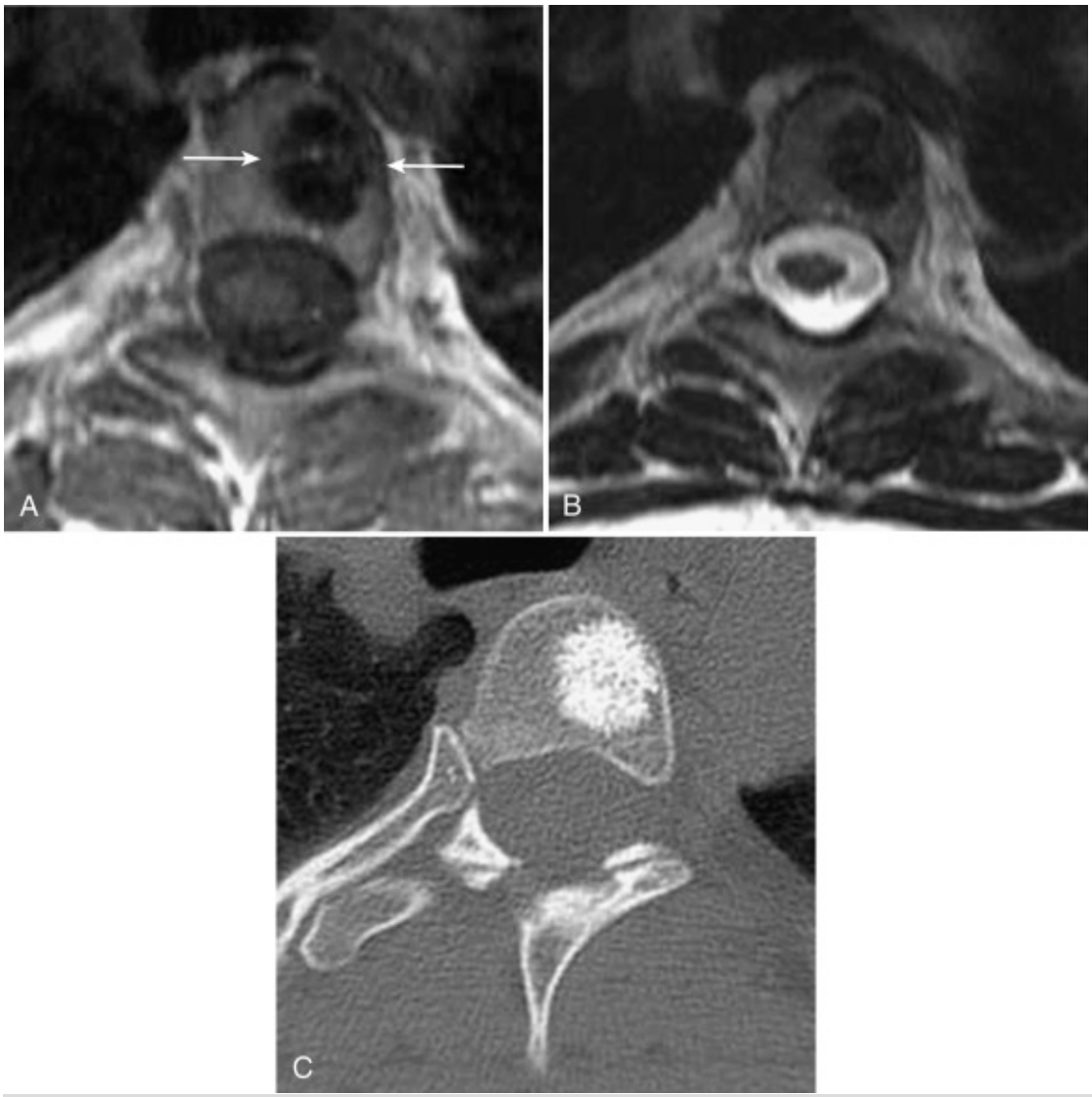

Fig. 7.15

Low signal intensity, T2: large bone island (enostosis). **A** , T1 axial image of the thoracic spine. An ovoid focus of extremely low signal intensity is seen in the T4 vertebral body (*arrows*). **B** , Fast spin echo–T2 axial image of the thoracic spine. The lesion remains extremely low signal intensity, confirming its sclerotic nature. **C** , CT scan of the thoracic spine. The dense sclerosis and typical spiculated margins of this large bone island are better shown.

Fibrous Lesions

Fibrous tissue is usually of low to intermediate signal intensity on T2W images, but fibrous lesions of bone often show variable MRI features.

A xanthofibroma (fibrous cortical defect, nonossifying fibroma) is a benign osseous lesion found in adolescents and young adults. These are readily diagnosed on conventional radiographs but may be incidentally detected on MR images. They display intermediate to low signal intensity on T1W images and often show low to intermediate signal on T2W images because of their fibrous nature. Increased signal also may be seen on T2W images, however, along with variable degrees of enhancement after gadolinium administration. Their lobular contour, eccentric location, low signal intensity, and sclerotic margin are helpful distinguishing features.

Similarly, it was suggested in the early MRI literature that fibrous dysplasia displays decreased signal intensity on T1W and T2W images because of its predominantly fibrous nature. This lesion does not have a characteristic appearance on MR images, however, and often shows heterogeneous signal intensity that may be high, low, or mixed on T2W images due to the different tissue types that can be seen within this lesion (Fig. 7.16 (f0085)).

Fig. 7.16

Fibrous dysplasia. **A** , Anteroposterior radiograph shows typical findings of fibrous dysplasia in the proximal tibia, with a long, mildly expansile lytic lesion that shows a hazy internal matrix. **B** , STIR coronal image of the proximal tibia. Most of the lesion shows homogeneous, mildly increased signal intensity, with a focus of higher signal intensity cystic change centrally **(C).**

(From Higgins CB, Hricak H, Helms CA [eds]. *Magnetic Resonance Imaging of the Body* . 3rd ed. Philadelphia: Lippincott-Raven; 1997.)

Primary Lymphoma of Bone

Primary lymphoma of bone is often of low signal intensity on T2W images, although its appearance varies (Fig. 7.17 (f0090)). Some investigators have found that the low signal intensity tissue corresponds to areas of fibrosis on pathologic analysis.

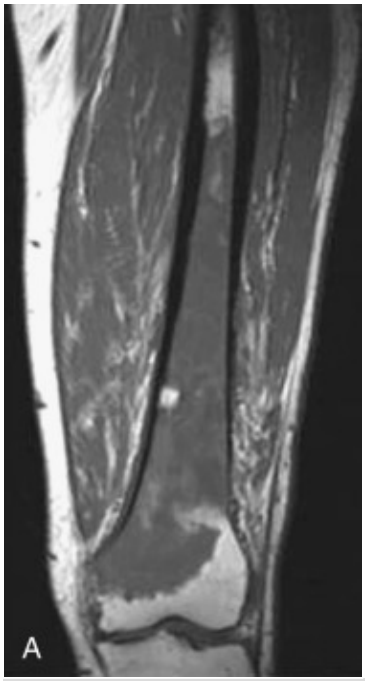

Fig. 7.17

Low signal intensity, T2: lymphoma of bone. **A** , T1 coronal image of the distal femur. Extensive, abnormal low signal intensity is present throughout the mid-to-distal portion of the femur. **B** , STIR coronal image of the distal femur. Much of the lesion shows markedly increased signal intensity, but a broad, bandlike area of low signal intensity persists distally (*arrowheads*). Biopsy revealed B cell lymphoma.

Fluid-Fluid Levels

The classic MRI appearance of an aneurysmal bone cyst is that of an expansile, lobular mass that contains multiple cystlike collections and shows high signal intensity on T2W images. Fluid-fluid levels are usually present within these cavities and correspond to stagnant blood products within the cavernous spaces that make up these lesions (Fig. 7.18 (f0095)). Initially, fluid-fluid levels were thought to be specific for an aneurysmal bone cyst, but they are a nonspecific feature of many entities that contain collections of blood, including telangiectatic osteosarcoma, chondroblastoma, giant cell tumor of bone, fibrous dysplasia, malignant fibrous histiocytoma of bone, and others. Also, because an aneurysmal

bone cyst may arise within some of these aforementioned lesions, such as telangiectatic osteosarcoma or giant cell tumor (secondary aneurysmal bone cyst), the presence of an associated mass indicates a biopsy is necessary. In an aneurysmal bone cyst, nonenhancing spaces should fill the entire lesion, allowing it to be distinguished from a secondary aneurysmal bone cyst.

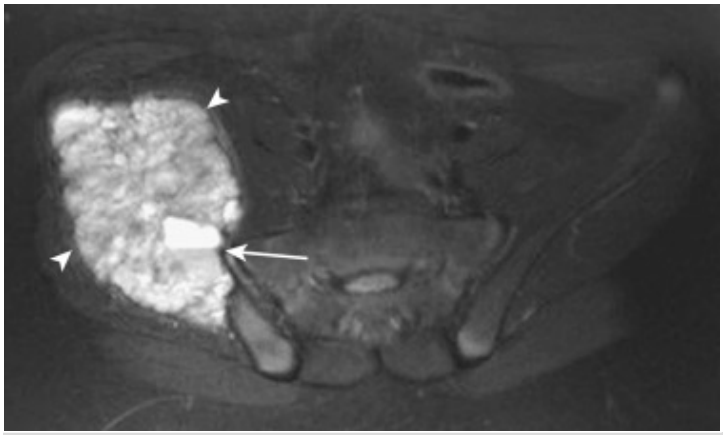

Fig. 7.18

Fluid-fluid levels: aneurysmal bone cyst. STIR axial image of the pelvis. The markedly expansile lesion (*arrowheads*) in the right iliac bone of this 10-year-old boy shows diffusely increased signal intensity and a prominent fluid-fluid level (*arrow*). Subsequent biopsy revealed this to be an aneurysmal bone cyst.

There is some evidence that the degree of involvement of a lesion with fluid-fluid levels may be helpful in differentiating benign from malignant lesions. In one investigation, if fluid-fluid levels made up more than two thirds of the lesion, it was found to be benign, most commonly an aneurysmal bone cyst. Conversely, in most malignant lesions, fluid-fluid levels made up less than one third of the mass.

Cartilaginous Tumors (Box 7.4 (b0025))

Enchondroma/Chondrosarcoma

An enchondroma displays a distinctive MRI appearance. This benign tumor is composed of multiple lobules that show homogeneously high signal intensity on T2W or STIR images with stippled areas of low signal, usually separated by thin, low signal intensity septa (Fig. 7.19 (f0100)). The increased signal intensity corresponds to the high water content of the hyaline cartilage lobules that compose these lesions. The low signal intensity foci correspond to calcified cartilage matrix. A pattern of enhancing rings and arcs is seen in cartilaginous tumors on postcontrast images, presumably caused by the presence of vessels within the fibrous septa and lack of cartilage enhancement. This MRI appearance, including the enhancement pattern, can be seen in enchondromas and low-grade chondrosarcomas.

BOX 7.4

MRI Features of Cartilage Tumors

- High signal lobules (cartilage) on T2 separated by thin, low signal septa
- Low signal intensity foci on T1W and T2W images (calcified cartilage matrix)
- Arcs and rings enhancement pattern
- Often impossible to distinguish enchondroma from low-grade chondrosarcoma
    - Watch out for features suggesting chondrosarcoma
    - Endosteal scalloping greater than two thirds of cortex
    - Cortical destruction and soft tissue mass

- Edema in adjacent marrow or soft tissues

Fig. 7.19

Enchondroma. **A** , T1 sagittal image of the distal femur. A lobular intramedullary mass is present in the distal femoral shaft. **B** , STIR coronal image of the distal femur. The lesion shows typical features of an enchondroma, including predominantly high signal intensity, lobular margins, thin internal septations, and low signal foci related to the chondroid matrix. Note also the lack of surrounding marrow edema.

Imaging findings suggestive of chondrosarcoma, rather than a benign enchondroma, include deep endosteal scalloping (more than two thirds of the cortex), cortical destruction with or without an associated soft tissue mass, and edema-like signal intensity in the adjacent marrow cavity and overlying soft tissues on STIR images Even so, it is often difficult, if not impossible, to distinguish between benign and low-grade malignant cartilaginous tumors based on imaging features alone.

Chondroid Tumor versus Medullary Bone Infarct

Differentiation of a cartilaginous tumor from a medullary bone infarct can be challenging on conventional radiographs because the chondroid matrix can appear similar to the dystrophic calcifications present within an area of infarction. These can easily be distinguished using MRI. In contrast to the cartilaginous lobules that make up the chondroid tumor, a medullary infarct is seen as a

flame-shaped region of heterogeneous signal intensity, often containing fat that is surrounded by a serpentine margin of low signal intensity on all sequences.

Osteochondroma

Osteochondroma is the most common benign tumor of bone and usually is diagnosed on conventional radiographs. MRI can differentiate an osteochondroma from other juxtacortical lesions by showing contiguity of the lesion's medullary cavity and cortex with those of the bone of origin. The marrow fat within the lesion should be isointense with the medullary fat of the host bone on all sequences. The cartilage cap of the lesion is easily detected because of its high signal intensity on T2W or STIR images (Fig. 7.20 (f0105)). Although the relationship between the thickness of the cap and malignancy is controversial, a thickness of more than 2 cm should be viewed as suspicious for neoplastic degeneration.

Fig. 7.20

Osteochondroma causing neuritis. **A** , T1 axial image of the proximal tibia. A large, pedunculated osteochondroma arises from the posterior tibia (T). Note the continuity of cortical margins and medullary cavities of the lesion and parent bone and the normal marrow signal intensity within the proximal lesion and tibia. **B** , STIR axial image of the proximal tibia. The high signal intensity and thin cartilage cap is amply displayed (*arrowheads*), as are high signal cartilaginous foci within the lesion. **C** , STIR axial image of the tibia (4 cm distal to **B**). The tibial nerve is focally enlarged (*arrow*) and shows increased signal intensity where it abuts the osteochondroma. Mechanical irritation resulted in a focal neuritis.

MRI can also show other symptomatic complications of these tumors, such as neurovascular impingement, bursal formation, or fracture (see Fig. 7.20 (f0105)).

Soft Tissue Tumors

General Principles

Some soft tissue tumors can be diagnosed with certainty based on their MRI signal characteristics; helpful differential MRI features are discussed subsequently. There is a large degree of overlap, however, in the MRI appearance of many benign and malignant soft tissue masses. For masses that have a nonspecific, indeterminate MRI appearance, a differential diagnosis can be generated using the patient's age, the location of the mass, and the information found in Tables 7.2 (t0015) and 7.3 (t0020) . For most lesions, a reasonable differential diagnosis would include the top three benign and top three malignant tumors listed in Tables 7.2 (t0015) and 7.3 (t0020) for a given age and location, but most indeterminate soft tissue masses

should be biopsied. The number of lesions in the tables should provide a sense of the significant imaging overlap of benign and malignant lesions.

Table 7.2

Distribution of Common Benign Soft Tissue Tumors by Anatomic Location and Age

From Kransdorf MJ. Benign soft-tissue tumors in a large referral population: distribution of specific diagnoses by age, sex, and location. *AJR Am J Roentgenol* . 1995;164:395-402. Reprinted with permission from the American Journal of Roentgenology.

Ages (yr)	Hand and Wrist	No. (%)	Upper Extremity	No. (%)	Axilla and Shoulder
0-5	Hemangioma	15 (15) * (tf0010)	Fibrous hamartoma infancy	15 (16)	Fibrous hamartoma infancy
	Granuloma annulare	14 (14)	Granuloma annulare	15 (16)	Hemangioma
	Infantile fibromatosis	13 (13)	Hemangioma	14 (15)	Lipoblastoma
	Infantile digital fibroma	8 (8)	Infantile fibromatosis	12 (13)	Fibrous hamartoma
	Fibromatosis	8 (8)	Fibrous histiocytoma	6 (6)	Myofibromato

Ages (yr)	Hand and Wrist	No. (%)	Upper Extremity	No. (%)	Axilla and Shoulder
	Aponeurotic fibroma	7 (7)	Juvenile xanthogranuloma	6 (6)	Lymphangiom
	Fibrous histiocytoma	5 (5)	Myofibromatosis	6 (6)	Nodular fasciit
	Other	27 (28)	Other	20 (21)	Other
6-15	Fibrous histiocytoma	32 (14)	Fibrous histiocytoma	41 (23)	Fibrous histiocytoma
	Hemangioma	31 (13)	Nodular fasciitis	39 (21)	Nodular fasciit
	Aponeurotic fibroma	25 (11)	Hemangioma	24 (13)	Hemangioma
	Fibroma tendon sheath	22 (9)	Granuloma annulare	12 (7)	Granular cell tumor
	GCT tendon sheath	17 (7)	Fibromatosis	11 (6)	Neurofibroma
	Fibromatosis	13 (6)	Neurofibroma	7 (4)	Lymphangiom
	Lipoma	9 (4)	Neurothekeoma	6 (3)	Myofibromato
	Other	86 (37)	Other	42 (23)	Other
16-25	GCT tendon sheath	84 (20)	Nodular fasciitis	130 (35)	Fibrous histiocytoma
	Fibrous histiocytoma	57 (14)	Fibrous histiocytoma	87 (23)	Nodular fasciit

Ages (yr)	Hand and Wrist	No. (%)	Upper Extremity	No. (%)	Axilla and Shoulder
	Fibroma tendon sheath	40 (10)	Neurofibroma	24 (6)	Lipoma
	Nodular fasciitis	26 (6)	Granuloma annulare	20 (5)	Neurofibroma
	Granuloma annulare	21 (5)	Granular cell tumor	17 (5)	Hemangioma
	Ganglion	20 (5)	Schwannoma	11 (3)	Schwannoma
	Other	132 (31)	Other	51 (14)	Other
26-45	Fibrous histiocytoma	167 (18)	Nodular fasciitis	309 (38)	Lipoma
	GCT tendon sheath	148 (16)	Fibrous histiocytoma	145 (18)	Fibrous histiocytoma
	Fibroma tendon sheath	106 (11)	Angiolipoma	48 (6)	Nodular fasciit
	Hemangioma	86 (10)	Hemangioma	43 (5)	Fibromatosis
	Nodular fasciitis	79 (8)	Schwannoma	43 (5)	Hemangioma
	Fibromatosis	46 (5)	Neurofibroma	37 (5)	Neurofibroma
	Chondroma	42 (4)	Lipoma	32 (4)	Schwannoma

Ages (yr)	Hand and Wrist	No. (%)	Upper Extremity	No. (%)	Axilla and Shoulder
46-65	GCT tendon sheath	143 (23)	Nodular fasciitis	86 (20)	Lipoma
	Fibrous histiocytoma	63 (10)	Lipoma	80 (19)	Fibrous histiocytoma
	Hemangioma	61 (10)	Fibrous histiocytoma	44 (10)	Myxoma
	Lipoma	59 (9)	Schwannoma	30 (7)	Fibromatosis
	Chondroma	52 (8)	Neurofibroma	24 (6)	Nodular fasciit
	Fibromatosis	43 (7)	Myxoma	24 (6)	Schwannoma
	Fibroma tendon sheath	37 (6)	Hemangioma	19 (4)	Granular cell tumor
	Other	172 (27)	Other	125 (29)	Other
≥ 66	GCT tendon sheath	51 (21)	Lipoma	39 (22)	Lipoma
	Hemangioma	24 (10)	Myxoma	19 (11)	Myxoma
	Schwannoma	24 (10)	Nodular fasciitis	18 (10)	Schwannoma
	Chondroma	24 (10)	Schwannoma	17 (9)	Fibromatosis

Ages (yr)	Neurofibroma and Wrist	No. (%)	Upper Extremity	No. (%)	Axilla and Shoulder
	Fibromatosis	14 (6)	Neurofibroma	10 (6)	Proliferative fasciitis
	Lipoma	13 (5)	Angiolipoma	10 (6)	Hemangioma
	Other	71 (29)	Other	55 (31)	Other

Ages (yr)	Hip, Groin, and Buttocks	No. (%)	Head and Neck	No. (%)	Trunk
0-5	Fibrous hamartoma infancy	14 (20)	Nodular fasciitis	47 (20)	Hema
	Lipoblastoma	14 (20)	Hemangioma	43 (18)	Juver xanth
	Myofibromatosis	8 (11)	Myofibromatosis	27 (11)	Myofi
	Lymphangioma	7 (10)	Fibromatosis	17 (7)	Nodu
	Fibrous histiocytoma	5 (7)	Granuloma annulare	14 (6)	Lipob
	Nodular fasciitis	4 (6)	Fibrous histiocytoma	13 (5)	Infant fibron
	Infantile fibromatosis	4 (6)	Infantile fibromatosis	13 (5)	Fibrou hama infanc
	Other	14	Other	63	Other

Ages (yr)	Hip, Groin, and Buttocks	No. (%)	Head and Neck	No. (%)	Trunk
	Other	14 (20)	Other	63 (27)	Other
6-15	Nodular fasciitis	15 (27)	Nodular fasciitis	75 (33)	Nodu
	Fibroma	7 (13)	Fibrous histiocytoma	34 (15)	Fibrou histio
	Fibrous histiocytoma	6 (11)	Neurofibroma	23 (10)	Hema
	Fibromatosis	5 (9)	Hemangioma	21 (9)	Lipom
	Lipoma	5 (9)	Myofibromatosis	14 (6)	Neuro
	Lipoblastoma	3 (5)	Fibromatosis	12 (5)	Fibro
	Neurofibroma	3 (5)	Lipoma	6 (3)	Granu tumo
	Other	11 (20)	Other	43 (19)	Other
16-25	Neurofibroma	20 (16)	Nodular fasciitis	61 (21)	Nodu
	Fibromatosis	18 (15)	Hemangioma	48 (17)	Fibro
	Fibrous histiocytoma	18 (15)	Fibrous histiocytoma	45 (16)	Fibrou histio
	Nodular fasciitis	12 (10)	Neurofibroma	37 (13)	Hema
	Hemangioma	9 (7)	Schwannoma	19 (7)	Neuro

Ages (yr)	Hip, Groin, and Buttocks	No. (%)	Head and Neck	No. (%)	Trunk
	Lipoma	8 (7)	Fibromatosis	11 (4)	Lipom
	Hemangiopericytoma	8 (7)	Lipoma	10 (4)	Schw
	Other	29 (24)	Other	56 (19)	Other
26-45	Lipoma	57 (17)	Lipoma	168 (22)	Lipom
	Neurofibroma	38 (12)	Nodular fasciitis	145 (19)	Nodu
	Fibrous histiocytoma	37 (11)	Fibrous histiocytoma	137 (18)	Fibro
	Fibromatosis	36 (11)	Hemangioma	97 (13)	Fibrou histio
	Nodular fasciitis	31 (9)	Neurofibroma	57 (8)	Hema
	Hemangiopericytoma	24 (7)	Hemangiopericytoma	37 (5)	Neuro
	Myxoma	22 (7)	Schwannoma	27 (4)	Schw
	Other	83 (25)	Other	91 (12)	Other
46-65	Lipoma	76 (35)	Lipoma	306 (46)	Lipom
	Myxoma	36 (17)	Nodular fasciitis	66 (10)	Fibro
	Fibrous histiocytoma	17 (8)	Hemangioma	55 (8)	Nodu

Ages (yr)	Hip, Groin, and Buttocks	No. (%)	Head and Neck	No. (%)	Trunk
	Schwannoma	17 (8)	Fibrous histiocytoma	42 (6)	Hema
	Nodular fasciitis	11 (5)	Neurofibroma	30 (4)	Fibrou histio
	Hemangiopericytoma	11 (5)	Schwannoma	25 (4)	Neuro
	Hemangioma	9 (4)	Myxoma	23 (3)	Schw
	Other	40 (18)	Other	120 (18)	Other
≥ 66	Lipoma	22 (21)	Lipoma	8 (50)	Lipom
	Myxoma	16 (15)	Hemangioma	22 (7)	Fibror
	Neurofibroma	13 (12)	Schwannoma	18 (6)	Neuro
	Schwannoma	10 (9)	Fibrous histiocytoma	17 (5)	Schw
	Hemangiopericytoma	10 (9)	Neurofibroma	16 (5)	Elasto
	Hemangioma	8 (8)	Nodular fasciitis	13 (4)	Myxo
	Nodular fasciitis	4 (4)	Myxoma	12 (4)	Hema
	Other	23 (22)	Other	58 (18)	Other

GCT , Giant cell tumor; *PVNS* , pigmented villonodular synovitis.

* 15 (15) indicates there were 15 hemangiomas in the hand and wrist of patients 0-5 years, and this represents 15% of all benign tumors in this location and age group.

Table 7.3

Distribution of Common Malignant Soft Tissue Tumors by Anatomic Location and Age

From Kransdorf MJ. Malignant soft-tissue tumors in a large referral population: distribution by age, sex, and location. *AJR Am J Roentgenol* . 1995;164:129-134. Reprinted with permission from the American Journal of Roentgenology.

Ages (yr)	Hand and Wrist	No. (%)	Upper Extremity	No (%)
0-5	Fibrosarcoma	5 (45) * (tf0015)	Fibrosarcoma	9 (29
	Angiosarcoma	1 (9)	Rhabdomyosarcoma	7 (23
	Epithelioid sarcoma	1 (9)	Angiomatoid MFH	3 (10
	Malignant GCT tendon sheath	1 (9)	DFSP	2 (6)
	DFSP	1 (9)	Giant cell fibroblastoma	2 (6)
	MPNST	1 (9)	MPNST	2 (6)

Ages (yr)	Rhabdomyosarcoma	No. (%)	Upper Extremity	No. (%)
			Other	4 (13
6-15	Epithelioid sarcoma	9 (21)	Angiomatoid MFH	30 (33
	Angiomatoid MFH	7 (16)	Synovial sarcoma	14 (15
	Synovial sarcoma	5 (12)	Fibrosarcoma	8 (9)
	MFH	4 (9)	MPNST	7 (8)
	Angiosarcoma	3 (7)	MFH	7 (8)
	Rhabdomyosarcoma	3 (7)	Rhabdomyosarcoma	7 (8)
	Clear cell sarcoma	2 (5)	Epithelioid sarcoma	4 (4)
	Other	10 (23)	Other	15 (16
16-25	Epithelioid sarcoma	25 (29)	Synovial sarcoma	32 (23
	MFH	11 (13)	MFH	19 (14
	DFSP	7 (8)	MPNST	16 (12
	Synovial sarcoma	7 (8)	Fibrosarcoma	12 (9)

Ages (yr)	Rhabdomyosarcoma	No. (%)	Liposarcoma	No. (%)
	Angiomatoid MFH	5 (6)	Epithelioid sarcoma	9 (7)
	Hemangioendothelioma	5 (6)	Hemangioendothelioma	6 (4)
	Other	19 (22)	Other	34 (25
26-45	MFH	26 (18)	MFH	65 (28
	Epithelioid sarcoma	24 (16)	MPNST	29 (12
	Synovial sarcoma	21 (14)	Fibrosarcoma	25 (11
	Fibrosarcoma	17 (12)	Synovial sarcoma	23 (10
	Clear cell sarcoma	9 (6)	Liposarcoma	20 (8)
	Liposarcoma	9 (6)	DFSP	18 (8)
	MPNST	7 (5)	Epithelioid sarcoma	13 (6)
	Other	33 (23)	Other	43 (18
46-65	MFH	16 (19)	MFH	133 (46
	Synovial sarcoma	12 (14)	Liposarcoma	34 (12

Ages (yr)	Hand and Wrist	No. (%)	Upper Extremity	No. (%)
	Epithelioid sarcoma	7 (8)	Fibrosarcoma	18 (6)
	Liposarcoma	7 (8)	MPNST	17 (6)
	Chondrosarcoma	7 (8)	Synovial sarcoma	16 (5)
	Clear cell sarcoma	5 (6)	Hemangioendothelioma	9 (3)
	Other	22 (26)	Other	43 (15
≥ 66	MFH	28 (35)	MFH	183 (60
	Leiomyosarcoma	8 (10)	Liposarcoma	25 (8)
	Synovial sarcoma	6 (8)	Leiomyosarcoma	23 (8)
	Kaposi’s sarcoma	5 (6)	MPNST	20 (7)
	DFSP	4 (5)	Kaposi’s sarcoma	10 (3)
	MPNST	4 (5)	Fibrosarcoma	8 (3)
	Clear cell sarcoma	3 (4)	Angiosarcoma	6 (2)
	Other	21 (27)	Other	29 (10

Ages (yr)	Hip, Groin, and Buttocks	No. (%)	Head and Neck	No. (%)	Trunk
0-5	Fibrosarcoma	7 (32)	Fibrosarcoma	22 (37)	Fibrosa
	Giant cell fibroblastoma	3 (14)	Rhabdomyosarcoma	20 (33)	Giant c fibrobl
	Rhabdomyosarcoma	3 (14)	Malignant hemangiopericytoma	3 (5)	Rhabd
	DFSP	2 (9)	Alveolar soft part sarcoma	2 (3)	Angior
	MFH	2 (9)	DFSP	2 (3)	DFSP
	Leiomyosarcoma	1 (5)	MPNST	2 (3)	Ewing's
	Synovial sarcoma	1 (5)	Giant cell fibroblastoma	2 (3)	Neurob
	Other	3 (14)	Other	7 (12)	Other
6-15	Angiomatoid MFH	8 (21)	Rhabdomyosarcoma	17 (26)	Angior
	Synovial sarcoma	7 (19)	Fibrosarcoma	13 (20)	Fibrosa
	Rhabdomyosarcoma	6 (16)	Synovial sarcoma	7 (11)	Ewing's
	MFH	4 (11)	MPNST	6 (9)	DFSP
	Epithelioid sarcoma	2	MFH	6	MPNST

Ages (yr)	Hip, Groin, and Buttocks	No. (%)	Head and Neck	No. (%)	Trunk
	Epithelioid sarcoma	2	MFH	6	MPNS
	Fibrosarcoma	2 (5)	Angiomatoid MFH	4 (6)	Rhabd
	MPNST	2 (5)	DFSP	2 (3)	MFH
	Other	7 (18)	Other	10 (15)	Other
16-25	Synovial sarcoma	15 (18)	Fibrosarcoma	15 (17)	DFSP
	MPNST	13 (16)	DFSP	14 (16)	MFH
	Liposarcoma	8 (10)	MPNST	8 (9)	MPNS
	DFSP	6 (7)	Synovial sarcoma	8 (9)	Fibros
	MFH	6 (7)	Rhabdomyosarcoma	8 (9)	Synovi
	Rhabdomyosarcoma	5 (6)	MFH	7 (8)	Ewing’
	Leiomyosarcoma	4 (5)	Angiomatoid MFH	6 (7)	Angior
	Other	26 (31)	Other	23 (26)	Other
26-45	Liposarcoma	45 (18)	DFSP	59 (30)	DFSP
	DFSP	42 (17)	MPNST	27 (14)	MFH
	MFH	38	Liposarcoma	18	MPNS

Ages (yr)	Hip, Groin, and Buttocks	No. (%)	Head and Neck	No. (%)	Trunk
	MFH	38 (16)	Liposarcoma	18 (9)	MPNS
	Leiomyosarcoma	26 (11)	MFH	15 (8)	Liposa
	MPNST	15 (6)	Fibrosarcoma	14 (7)	Fibrosa
	Synovial sarcoma	13 (5)	Synovial sarcoma	10 (5)	Synovi
	Fibrosarcoma	12 (5)	Angiosarcoma	9 (4)	Angios
	Other	53 (22)	Other	42 (22)	Other
46-65	Liposarcoma	67 (24)	MFH	54 (28)	MFH
	MFH	66 (23)	DFSP	28 (15)	Liposa
	Leiomyosarcoma	40 (14)	MPNST	23 (12)	DFSP
	DFSP	20 (7)	Liposarcoma	22 (12)	MPNST
	Fibrosarcoma	16 (6)	Angiosarcoma	16 (8)	Leiomy
	Synovial sarcoma	14 (5)	Atypical fibroxanthoma	12 (6)	Fibrosa
	Chondrosarcoma	14 (5)	Leiomyosarcoma	11 (6)	Angios
	Other	46 (16)	Other	24 (13)	Other
> 66	MFH	111	MFH	82	MFH

≥ 66 Ages (yr)	MFH Hip, Groin, and Buttocks	111 No. (%)	MFH Head and Neck	82 No. (%)	MFH Trunk
	Liposarcoma	49 (20)	Atypical fibroxanthoma	41 (17)	Liposa
	Leiomyosarcoma	24 (10)	Angiosarcoma	27 (11)	Leiomy
	Angiosarcoma	11 (5)	Liposarcoma	20 (8)	MPNS
	MPNST	11 (5)	MPNST	16 (7)	DFSP
	Fibrosarcoma	10 (4)	Leiomyosarcoma	13 (5)	Fibrosa
	Chondrosarcoma	7 (3)	Fibrosarcoma	10 (4)	Chond
	Other	20 (8)	Other	31 (13)	Other

DFSP , Dermatofibrosarcoma protuberans; *GCT* , giant cell tumor; *MFH* , malignant fibrous histiocytoma; *MPNST* , malignant peripheral nerve sheath tumor.

* 5 (45) indicates there were 5 fibrosarcomas in the hand and wrist of patients 0-5 years, and this represents 45% of all malignant tumors in this location and age group.

Differential Features

High Signal on T1W Images (**Box 7.5** (b0030))

The differential diagnosis for lesions that contain areas of high signal intensity on T1W images is limited. This finding usually indicates fat or subacute blood products within the mass.

BOX 7.5

Soft Tissue Masses Containing High Signal on T1W Images

- Lipoma
- Liposarcoma
- Hematoma (subacute)
- Hemangioma
- Melanoma

Lipomatous Masses

A lipoma is a benign fatty tumor that displays a characteristic MRI appearance, allowing for a confident diagnosis. These generally are well-defined, lobular masses that show homogeneous signal intensity that parallels subcutaneous fat on all sequences (high signal intensity on T1W images and intermediate to high signal intensity on T2W images) (Fig. 7.21 (f0110)). Thin, curvilinear septations often course through the fatty mass and may enhance mildly after gadolinium administration. Most superficial lesions are well circumscribed, whereas deeper lesions may arise within muscle and appear more infiltrative (Fig. 7.22 (f0115)).

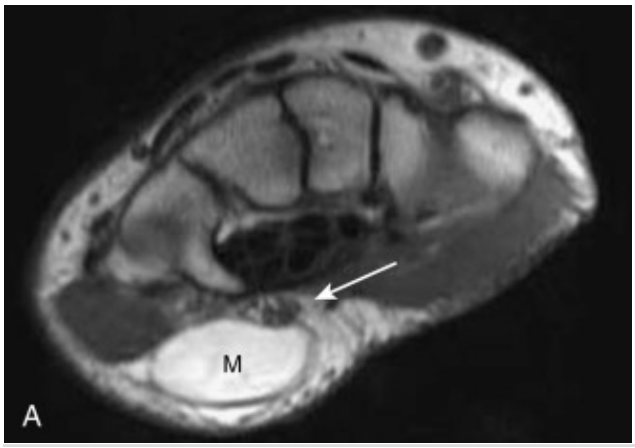

Fig. 7.21

High signal intensity, T1: soft tissue lipoma. **A** , T1 axial image of the wrist. A sharply circumscribed, high signal intensity mass (M) abuts and slightly compresses the ulnar neurovascular bundle (*arrow*) in this patient who presented with an ulnar neuropathy. **B** , T2 axial image with fat suppression of the wrist. With the exception of the thin internal septations, there is excellent suppression of the signal intensity from this mass, confirming its lipomatous nature. Subsequent resection revealed a benign lipoma.

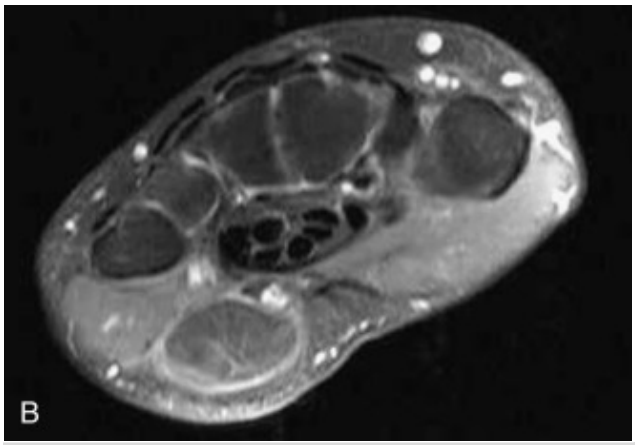

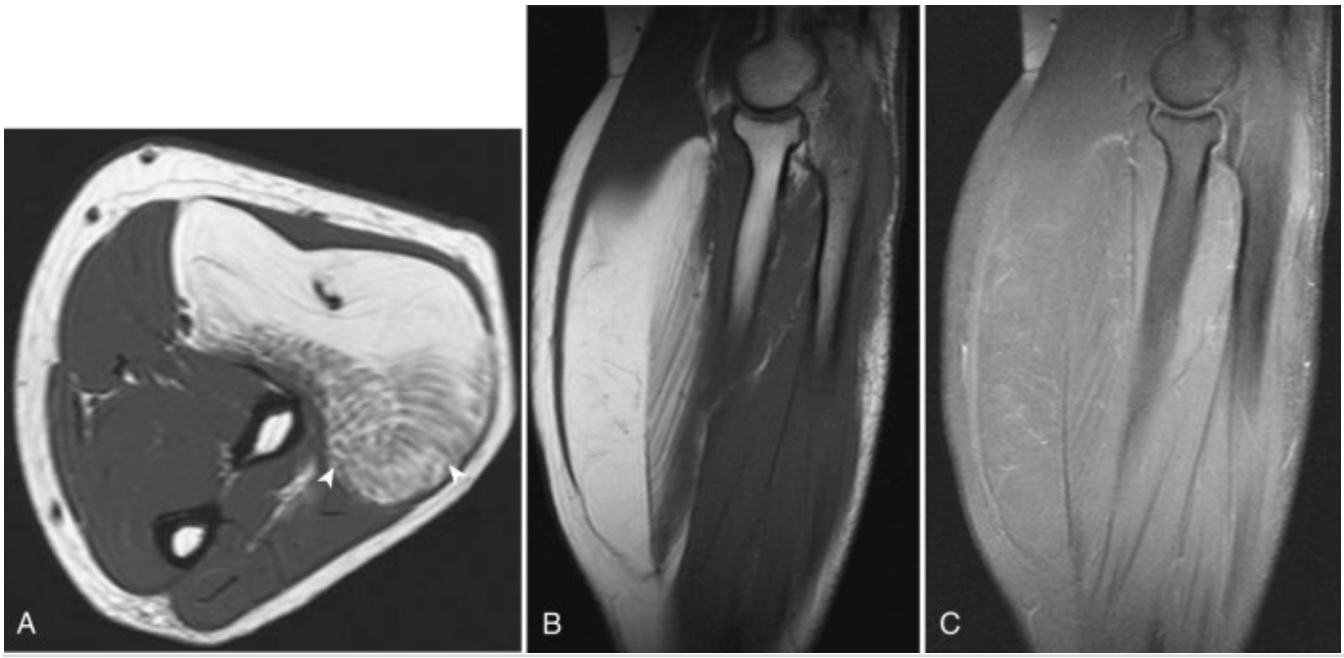

Fig. 7.22

High signal intensity, T1: intramuscular lipoma. **A** , T1 axial image of the forearm. A large, predominantly high signal intensity mass infiltrates the musculature of the mid-forearm. Note the feathery, intermediate signal intensity muscle fibers within the mass (*arrowheads*). **B** , T1 sagittal image of the forearm. The infiltration of muscle fibers is seen to better advantage in this plane. **C** , T1 fat-saturated sagittal image after gadolinium administration. There is complete saturation of the signal from the mass with the exception of some thin enhancing septations compatible with an intramuscular lipoma.

An atypical lipoma (well-differentiated liposarcoma) is considered a low-grade malignant tumor that tends to recur locally after surgery but does not metastasize. Histologically, these tumors are composed of mature adipose tissue and other nonfatty elements, often contained in thick, irregular septa. The MRI appearance of these lesions parallels their histology. They typically show a predominant fat signal with coarse, thickened septa or scattered areas of nonfatty tissue. The nonlipomatous elements show low signal intensity on

T1W images and high signal or enhancement on T2W or postgadolinium T1W images (Fig. 7.23 (f0120)). Gadolinium is not necessary to make the diagnosis of fat-containing lesions like lipomas or atypical lipomas.

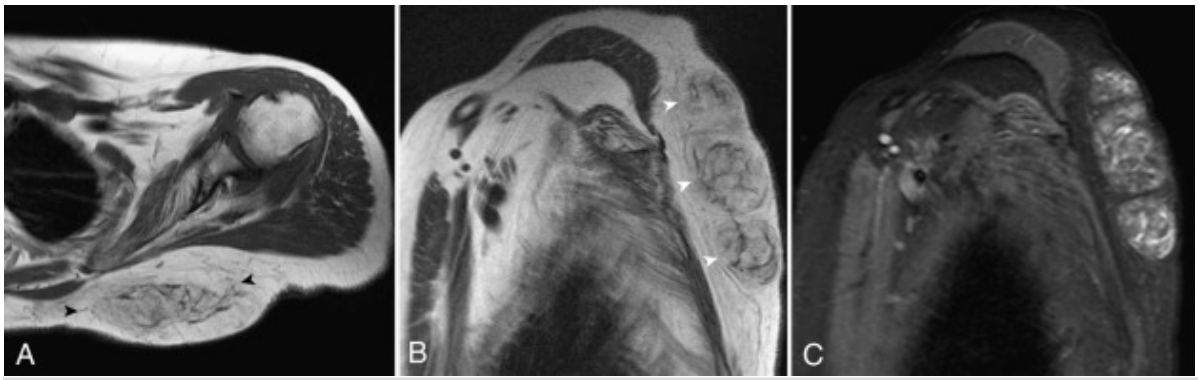

Fig. 7.23

High signal intensity, T1: atypical lipoma (well-differentiated liposarcoma). **A** , T1 axial image of the posterior chest wall. There is an ovoid mass of predominantly fat signal intensity within the soft tissues of the upper back (*arrowheads*). Note the hazy intermediate signal intensity and mildly thickened septa in the central portion of the mass. **B** , T1 sagittal image of the chest wall and axilla. There are at least three lobules within the mass showing similar architecture and signal intensity with areas of fat and nonlipomatous tissue (*arrowheads*). **C** , STIR sagittal image of the chest wall and axilla. There is heterogeneous signal intensity throughout the mass. Subsequent biopsy revealed an atypical lipoma.

There are several subtypes of liposarcomas. Myxoid liposarcoma is the most common and may appear benign on MR images. These gelatinous lesions often show a cystic appearance that is indistinguishable from other myxomatous tumors or even a simple cyst (Fig. 7.24 (f0125)). High-grade liposarcomas often contain no recognizable fat and are indistinguishable from other malignant soft tissue tumors.

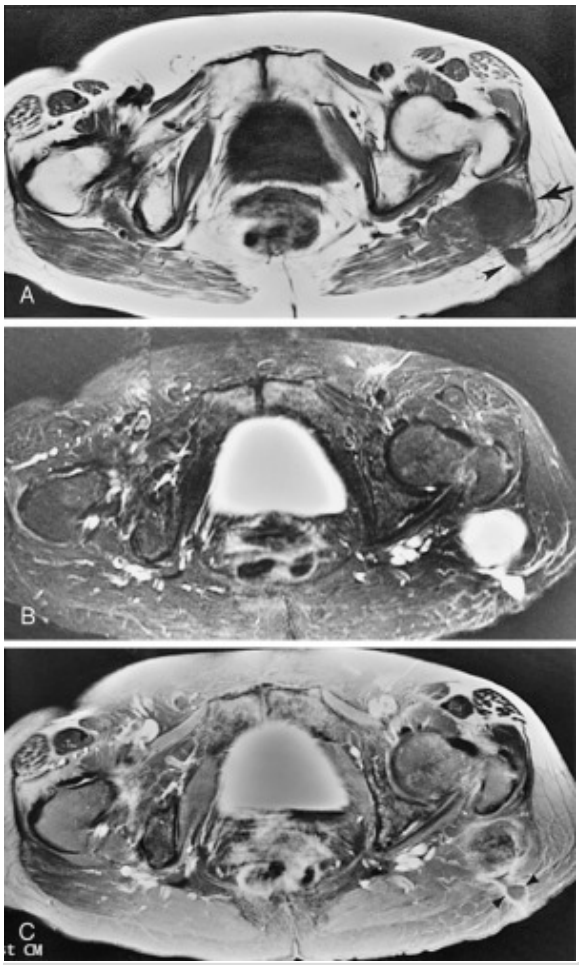

Fig. 7.24

Liposarcoma without fat evident. **A** , T1 axial image of the pelvis. There is a very low signal intensity, rounded mass in the left gluteal musculature (*arrow*). The low signal intensity within the subcutaneous fat (*arrowhead*) is related to a prior biopsy. **B** , STIR axial image of the pelvis. The mass shows homogeneously increased signal intensity and smooth margins. **C** , T1 axial image with fat saturation of the pelvis, after administration of IV gadolinium. The mass shows poorly defined, heterogeneous enhancement. Note the enhancement along the margins of the biopsy track and lack of enhancement of the central fluid within it (*arrowheads*).

Vascular Malformations

Vascular malformations are benign lesions that lie along a pathologic spectrum ranging from capillary and cavernous hemangiomas (containing variable amounts of nonvascular tissue,

such as fat, smooth muscle, or fibrous tissue) to true arteriovenous malformations that are composed of larger vessels. Regardless of the specific type of malformation, it is most important to recognize these as benign vascular lesions and to describe their extent and what anatomic structures they involve.

Cavernous hemangiomas usually display well-defined, lobular contours, although they may appear infiltrative by extending from one compartment to another, including infiltrating bone. On T1W images, they are predominantly isointense to muscle, but often show variable amounts of increased signal intensity related to fat content. Their very high signal intensity on T2W images reflects the stagnant blood within their cavernous spaces (Fig. 7.25 (f0130)). Scattered foci of decreased signal intensity, corresponding to calcified phleboliths, thrombosed channels, or septa seen on end, may also be seen on T2W images. The presence of fibrofatty tissue with scattered foci of low signal is diagnostic.

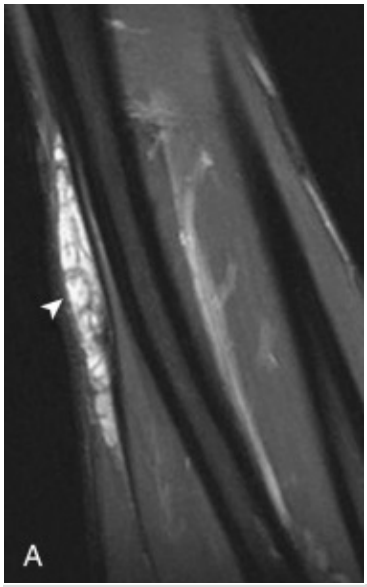

Fig. 7.25

High signal intensity, T1: soft tissue hemangioma. **A** , STIR coronal image of the forearm. There is an elongated mass in the superficial soft tissues of the mid-forearm (*arrowhead*), which shows lobules of increased signal and numerous septations. **B** , T1 coronal image of the forearm. The mass contains extensive fat between the lobular vascular channels, an appearance compatible with a soft tissue hemangioma.

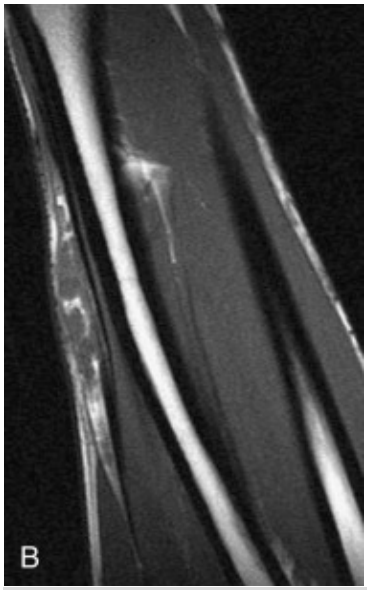

Arteriovenous malformations are composed of large, high-flow vessels, which result in dark intraluminal flow voids on T1W and T2W images and increased signal intensity on “flow-sensitive” gradient echo images (Fig. 7.26 (f0135)). Large feeding arteries and draining veins may also be evident in the adjacent soft tissues.

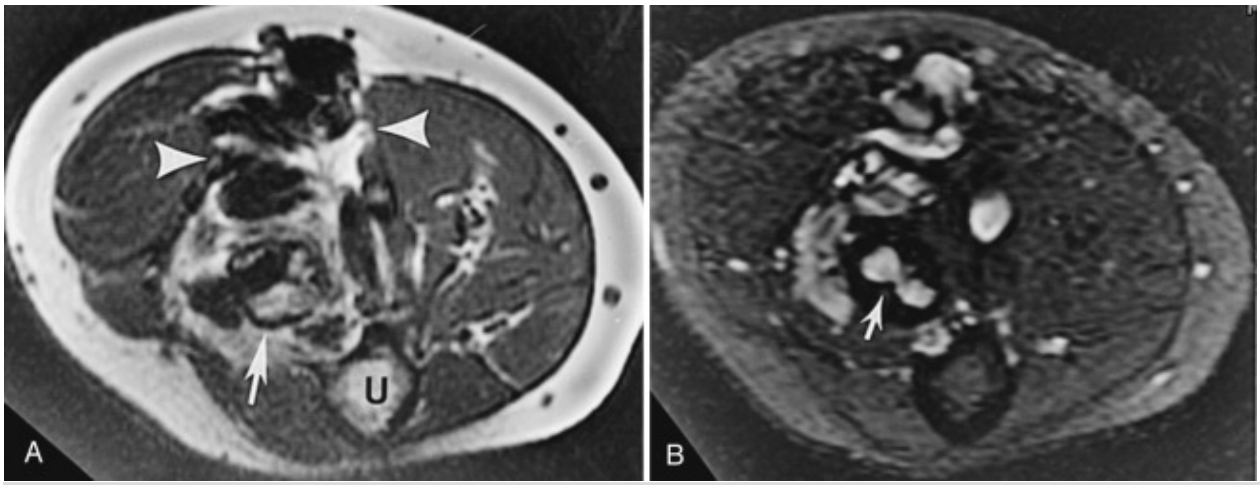

Fig. 7.26

High signal intensity, T1: arteriovenous malformation. **A** , T1 axial image of the proximal forearm. A palpable mass in the volar soft tissues of the proximal forearm (*arrowheads*) is shown to be made up of large, low signal intensity tubular structures interspersed with high signal intensity fat. *U* , Ulna. *Arrow* points to radius. **B** , T2* (gradient echo) axial image of the proximal forearm. Flow-related high signal intensity is seen within the large vessels making up this arteriovenous malformation on this “flow-sensitive” sequence. Note the direct extension into the proximal radius (*arrow*).

(From Higgins CB, Hricak H, Helms CA [eds]. *Magnetic Resonance Imaging of the Body* . 3rd ed. Philadelphia: Lippincott-Raven; 1997.)

Hematoma

Hemorrhage into soft tissues usually displays a heterogeneous, often laminated appearance. The signal characteristics of extracranial hemorrhage are less predictable than with intracranial bleeding, but an acute hematoma (roughly up to 1 week old) is typically isointense to skeletal muscle on T1W images and of lower signal intensity than muscle on T2W images. In subacute and chronic hematomas, areas of high signal intensity usually are evident on T1W images somewhere within the mass (Fig. 7.27 (f0140)). These areas may display increased or decreased signal intensity on T2W images. In more chronic hematomas, areas of hemosiderin deposition, typically along the periphery, show decreased signal intensity on T1W and T2W images.

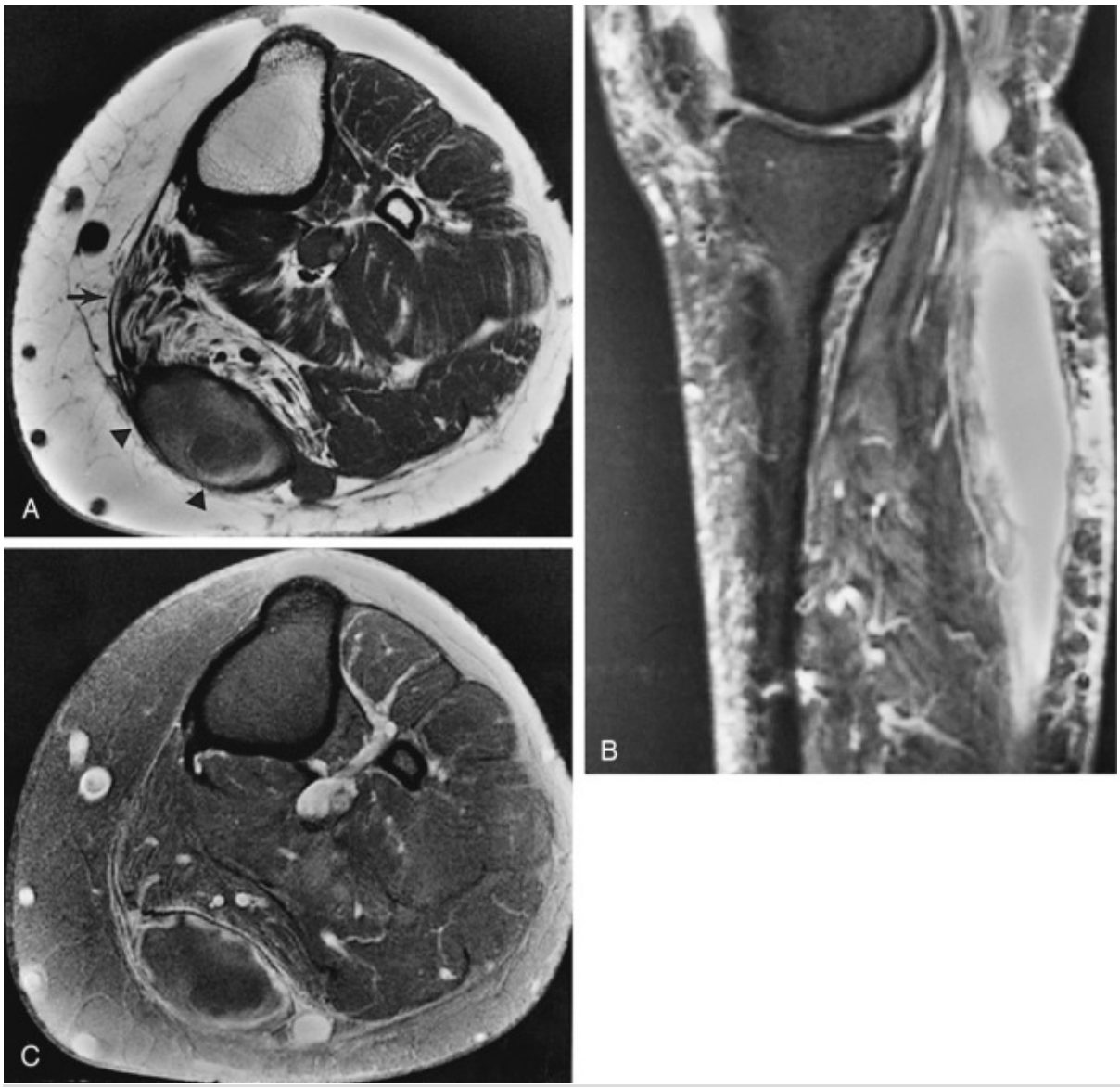

Fig. 7.27

High signal intensity, T1: hematoma. **A** , T1 axial image of the proximal calf. This well-circumscribed mass (*arrowheads*) shows mildly increased signal intensity compatible with subacute blood products surrounded by a low signal intensity rim. This hematoma could be traced back to the posteromedial knee joint, where it was seen to represent a hemorrhage within a Baker's cyst. Note also the fatty atrophy within the medial head of the gastrocnemius muscle (*arrow*). **B** , STIR sagittal image of the calf. The hematoma shows diffusely increased signal intensity. **C** , T1 axial image with fat saturation of the proximal calf. There is peripheral enhancement, but compared with the precontrast image, there is no significant enhancement centrally, indicating its cystic nature.

A hemorrhagic neoplasm can be indistinguishable from a hematoma related to other causes (Fig. 7.28 (f0145)). At a minimum, any hematoma detected with MRI must be followed to resolution, either clinically or with serial imaging. Gadolinium administration may reveal an enhancing tumor mass; however, this must be interpreted with caution because fibrovascular tissue within an organizing hematoma may also enhance. In questionable cases, image-guided biopsy should be considered.

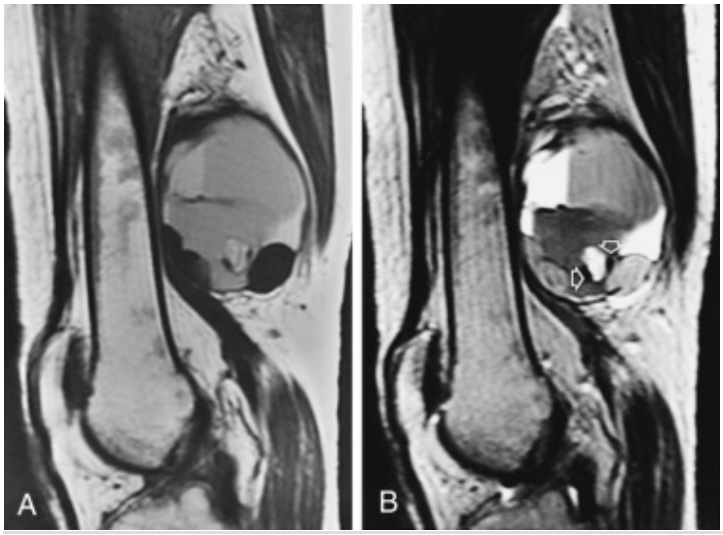

Fig. 7.28

High signal intensity, T1: hemorrhagic tumor. **A** , T1 sagittal image of the distal thigh. A large, heterogeneous mass is seen in the posterior compartment of the distal thigh. Note the multiple fluid-fluid levels and areas of high signal intensity compatible with subacute hemorrhage. **B** , T2 sagittal image of the distal thigh. The peripheral rim and internal foci (*open arrows*) of persistent low signal intensity are compatible with hemosiderin. Biopsy revealed hemorrhagic synovial sarcoma.

Melanoma

Malignant melanoma may show increased signal intensity on T1W images, presumably caused by the presence of paramagnetic compounds within the lesion. For the same reason, these tumors may display low signal intensity on T2W images (Fig. 7.29 (f0150)).

Fig. 7.29

High signal intensity, T1: melanoma. **A** , T1 coronal image of the pelvis. There is a large, lobular melanoma metastasis in the proximal adductor muscles of the left thigh showing extensive, increased signal intensity (*arrow*). **B** , STIR coronal image of the pelvis. Note the large foci of low signal intensity within the mass, presumably related to paramagnetic compounds.

Low Signal on T2W Images (Box 7.6 (b0035))

Pigmented Villonodular Synovitis

Pigmented villonodular synovitis (PVNS) is a synovial disease of unknown cause that most commonly affects the knee and results in an abnormal proliferation of histiocytes and giant cells, which usually contain hemosiderin. The most distinctive MRI features of this entity are masslike areas of synovial proliferation that show foci of low signal intensity on T1W and T2W images related to the hemosiderin (Fig. 7.30 (f0155)). A similar appearance may be seen

with chronic hemarthrosis, chronic rheumatoid arthritis, chronic infectious arthritis (e.g., tuberculosis), amyloidosis, or gout. The hemosiderin deposits are unique to PVNS, and when gradient echo imaging is performed, the areas of hemosiderin produce a characteristic "blooming" appearance (accentuation of the areas of dark signal intensity). As this is a synovial-based process, the entire joint needs to be evaluated to identify additional foci of involvement for appropriate treatment.

BOX 7.6

Soft Tissue Masses Containing Low Signal on T2W Images

- Pigmented villonodular synovitis/giant cell tumor of the tendon sheath
- Fibrous lesions
- Hematoma (chronic → hemosiderin)
- Amyloid
- Gout
- Melanoma

Fig. 7.30

Low signal intensity, T2: pigmented villonodular synovitis. **A** , T1 sagittal image of the knee. Extensive intermediate signal intensity fluid or tissue distends the knee joint, most prominently posteriorly (*arrowheads*) where numerous low signal intensity foci are present within it. **B** , T2*–gradient echo sagittal image of the knee. The masses remain of low signal intensity and show prominent “blooming” secondary to susceptibility effects of hemosiderin compatible with pigmented villonodular synovitis.

Giant Cell Tumor of the Tendon Sheath

An extra-articular form of PVNS is called *giant cell tumor of the tendon sheath* . This is typically a focal mass arising in proximity to a tendon and most commonly is found in the hand and wrist. Because of their similar histology to PVNS, these lesions display intermediate to low signal intensity on T1W images and heterogeneous signal intensity on T2W images, with areas of decreased signal related to hemosiderin (Fig. 7.31 (f0160)).

Fig. 7.31

Low signal intensity, T2: giant cell tumor of the tendon sheath. **A** , T1 sagittal image of the finger. An ovoid, predominantly low signal intensity mass abuts and slightly deforms the underlying flexor tendons. **B** , Fat-saturated T2 sagittal image of the finger. The mass remains of low signal intensity and contains areas of darker signal intensity that are more prominent on this sequence related to hemosiderin in this giant cell tumor of the tendon sheath (extra-articular pigmented villonodular synovitis).

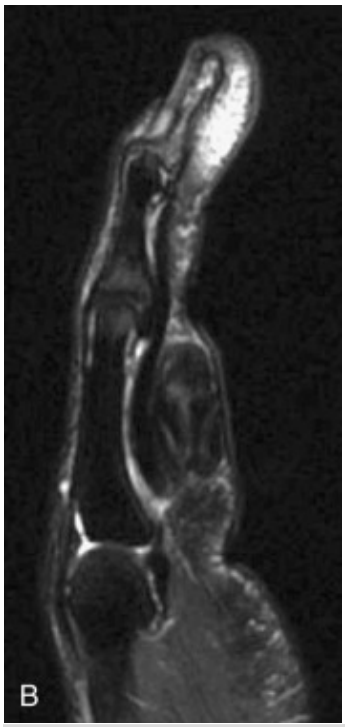

Fibrous Lesions

Soft tissue lesions containing predominantly fibrous tissue often show intermediate to low signal intensity on T2W images, at least in some portion of the mass (Fig. 7.32 (f0165)). Common entities include plantar fibroma (arising within the plantar aponeurosis); Morton's neuroma (a mass of perineural fibrosis surrounding a plantar digital nerve, most commonly between the third and fourth metatarsal heads); and desmoid tumors (benign but locally aggressive fibrotic lesions).

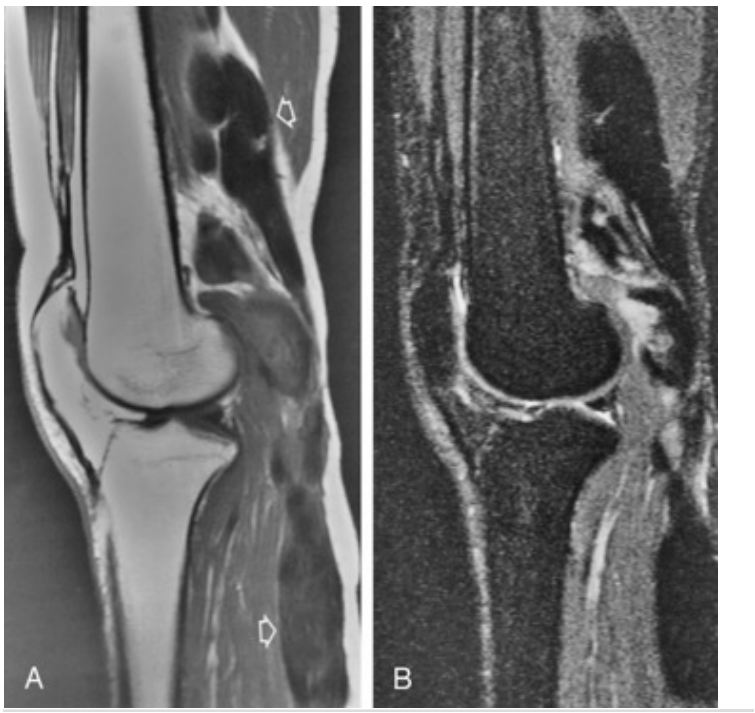

Fig. 7.32

Low signal intensity, T2: fibromatosis. **A** , Sagittal T1 image of the knee. Large, lobular, low signal intensity masses are seen in the soft tissues of the posterior distal thigh and proximal calf (*arrows*). **B** , STIR sagittal image of the knee. The masses remain of diffusely low signal intensity and were shown on subsequent biopsy to represent fibromatosis.

Amyloid

Amyloid is a protein-like substance that is deposited throughout musculoskeletal tissues as part of a primary disorder or related to other chronic diseases (secondary amyloidosis). The secondary form is most common in patients with end-stage renal disease who are undergoing hemodialysis. Amyloid deposition can occur in bone, intervertebral disk, or other soft tissues, with the hip and shoulder being the most commonly affected joints (Fig. 7.33 (f0170)). The tissue shows low to intermediate signal intensity on T1W and T2W images, probably caused by its collagen-like composition.

Fig. 7.33

Low signal intensity, T2: amyloid. **A** , T1 coronal image of the pelvis. Prominent low signal intensity tissue is seen within both hip joints (*arrows*). **B** , STIR coronal image of the pelvis. The tissue remains of relatively low signal intensity and is outlined by small bilateral joint effusions (*arrowheads*). The patient has a history of end-stage renal disease.

Gout

Gouty tophi also may show low to intermediate signal intensity on T1W and T2W images, with or without associated bone erosions. These signal characteristics may be related to fibrous tissue, hemosiderin deposition, or calcification.

Melanoma

Malignant melanoma shows variable signal intensities on MRI, but may display low signal intensity on T2W images, probably because of paramagnetic compounds within the tumor (see Fig. 7.29 (f0150)).

Cystic-Appearing Masses (Box 7.7 (b0040))

Cyst

Cystic lesions, such as fluid-filled bursae, synovial cysts, or ganglia, are common musculoskeletal masses. These often occur in typical locations such as the popliteal fossa or along the dorsum of the wrist, but may arise in unusual locations. A purely cystic mass shows homogeneous low signal intensity hypointense to muscle on T1W images and diffusely high signal on T2W images. Thin, low signal intensity septa are frequently present within ganglion cysts on T2W images. After IV gadolinium administration, there is enhancement of the thin, peripheral wall and internal septa, if present, with a lack of central enhancement (Fig. 7.34 (f0175)).

BOX 7.7

Cystic-Appearing Masses

- Cyst/ganglion
- Intramuscular myxoma
- Myxoid malignancy
  - Liposarcoma
  - Chondrosarcoma
  - Malignant fibrous histiocytoma

- Synovial sarcoma
- Nerve sheath tumor
- IV gadolinium can differentiate cystic/solid lesions

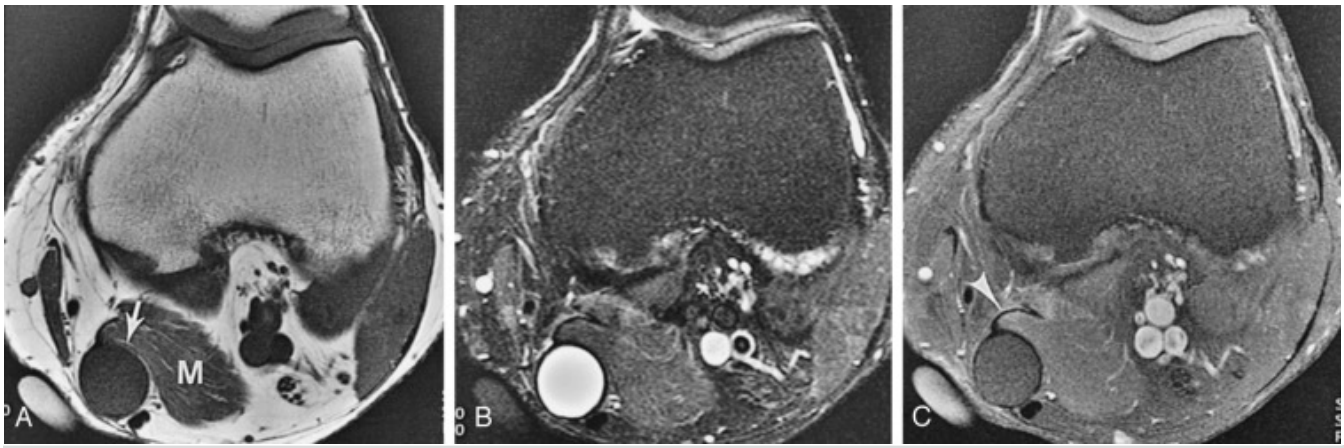

Fig. 7.34

Cyst. **A** , T1 axial image of the knee. There is a well-circumscribed mass in the posteromedial soft tissues (*arrow*) distorting the adjacent semimembranosus muscle (M). Note the homogeneous internal signal intensity, which is lower than that of the adjacent muscle. **B** , STIR axial image of the knee. The mass shows homogeneously increased signal intensity. **C** , T1 fat-suppressed axial image of the knee after administration of IV gadolinium. There is no enhancement of the mass, confirming the cystic nature of this ganglion, which appears to arise from the semimembranosus tendon (*arrowhead*).

Intramuscular Myxoma

These tumors are related to ganglion cysts and contain thick, gelatinous material that accounts for their cystic appearance on MRI. They are typically well-circumscribed lesions that are homogeneously hypointense to muscle on T1W images and diffusely hyperintense to fat on T2W images (Fig. 7.35 (f0180)).

After gadolinium administration, these usually show some peripheral or septal enhancement, although heterogeneous internal enhancement may be seen.

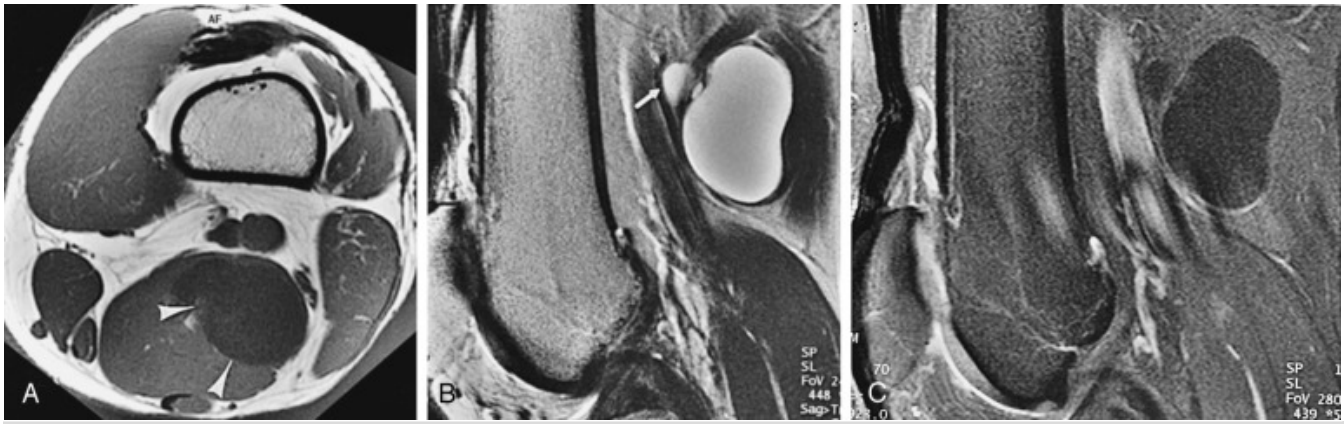

Fig. 7.35

Cystic-appearing lesion: myxoma. **A** , T1 axial image of the distal thigh. A low signal intensity mass (*arrowheads*) is arising within the semimembranosus muscle. Its internal signal intensity is lower than that of the surrounding muscle. **B** , Sagittal turbo spin echo–T2 image of the distal thigh. The mass shows homogeneously increased signal intensity. Note the anterior lobulation (*small arrow*). **C** , T1 fat-suppressed sagittal image of the knee after administration of IV gadolinium. There is no internal enhancement within this intramuscular myxoma.

Cystic-Appearing Malignant Tumors

Solid tumors that contain myxoid elements (myxoid liposarcoma, chondrosarcoma, malignant fibrous histiocytoma) or synovial sarcoma may show a cystic or predominantly cystic appearance (Figs. 7.36 (f0185) and 7.37 (f0190)). When a cystic-appearing lesion is identified in an atypical location and there is absence of the classic MRI features of a pure cyst (thin wall, homogeneous low signal intensity on T1W images, high signal on T2W images), evaluation with contrast enhancement is indicated. Contrast images may

indicate a solid portion of the lesion. Aspiration or biopsy should be done if there are any atypical features to differentiate a benign cyst or intramuscular myxoma from a malignant lesion.

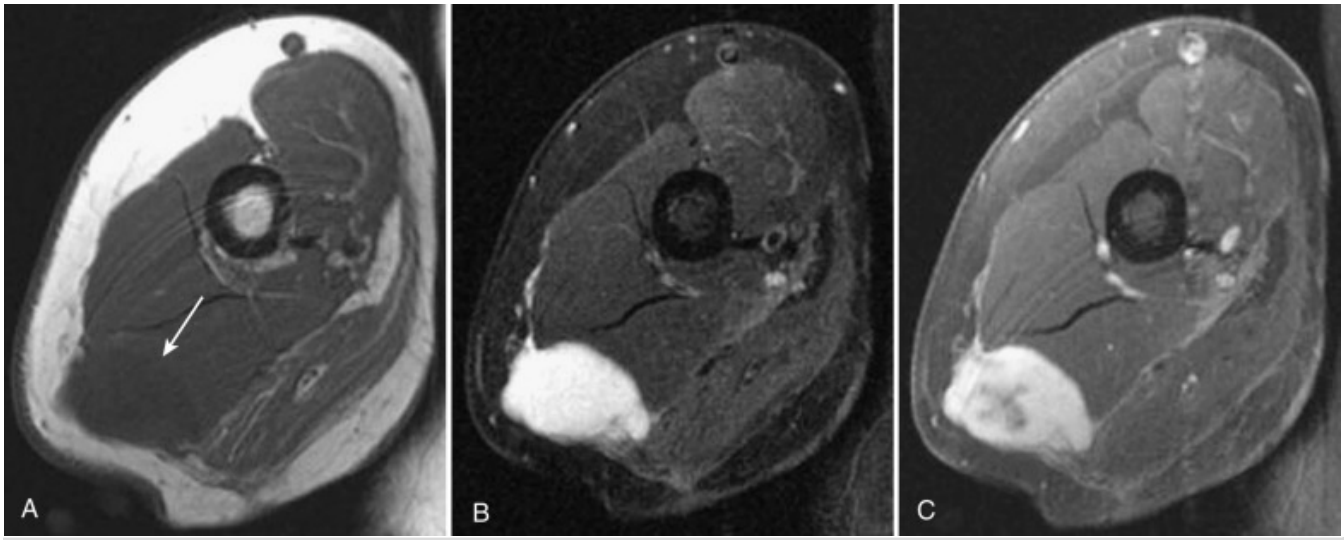

Fig. 7.36

Cystic-appearing lesion: myxofibrosarcoma. **A** , T1 axial image of the upper arm. An ovoid intermediate signal intensity mass is seen within the posterior soft tissues of the upper arm (*arrow*). **B** , STIR axial image of the upper arm. The mass shows homogeneous increased signal, suggesting a possible cystic mass. **C** , T1 fat-suppressed axial image of the upper arm after administration of IV gadolinium. The mass shows diffuse enhancement, confirming the noncystic nature of this recurrent myxofibrosarcoma.

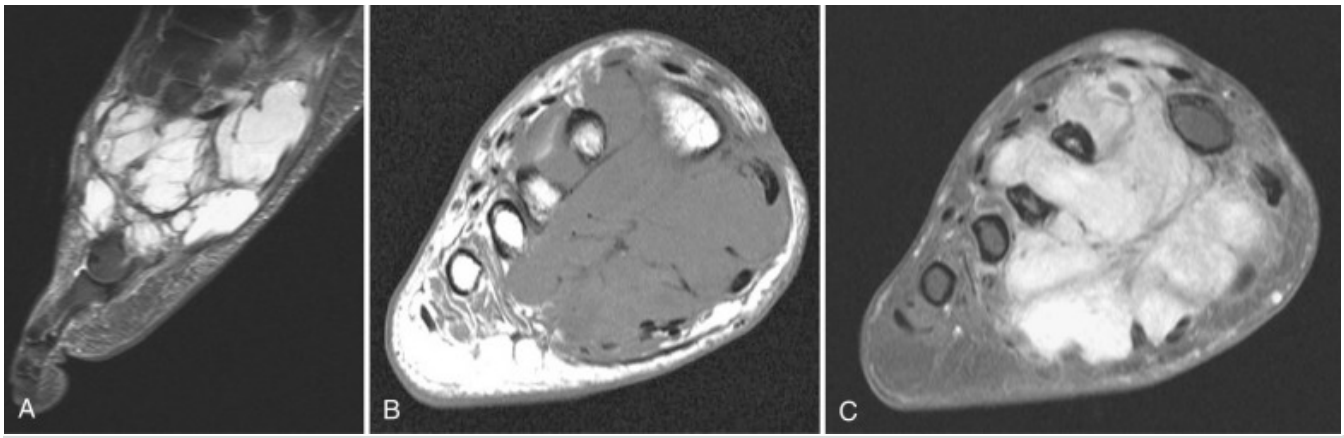

Fig. 7.37

Cystic-appearing lesion: synovial sarcoma. **A** , STIR sagittal image of the foot. A multilobular, high signal intensity mass extends throughout the midfoot. The homogeneous increased signal suggests a possible cystic mass. **B** , T1 axial image of the foot. The mass shows intermediate signal intensity, higher than expected for simple fluid. **C** , T1 fat-suppressed axial image of the foot after administration of IV gadolinium. The mass shows diffuse enhancement compatible with a solid mass—in this case, a synovial sarcoma.

Nerve Sheath Tumors

Peripheral nerve sheath tumors (schwannoma, neurofibroma) may have a cystic appearance because of their well-circumscribed margins and homogeneous high signal intensity on T2W images. MRI features suggesting the diagnosis of a nerve sheath tumor rather than a cyst include identification of the tubular-shaped nerve entering and exiting the mass (best seen on longitudinal images), the split-fat sign (a peripheral rim of fat surrounding the lesion), multiple small nerve fascicles within the lesion on T2W images, and the "target sign" on T2W images (higher signal in the periphery surrounding central lower signal intensity) (Fig. 7.38 (f0195)). These also typically show diffuse enhancement after IV administration of gadolinium.

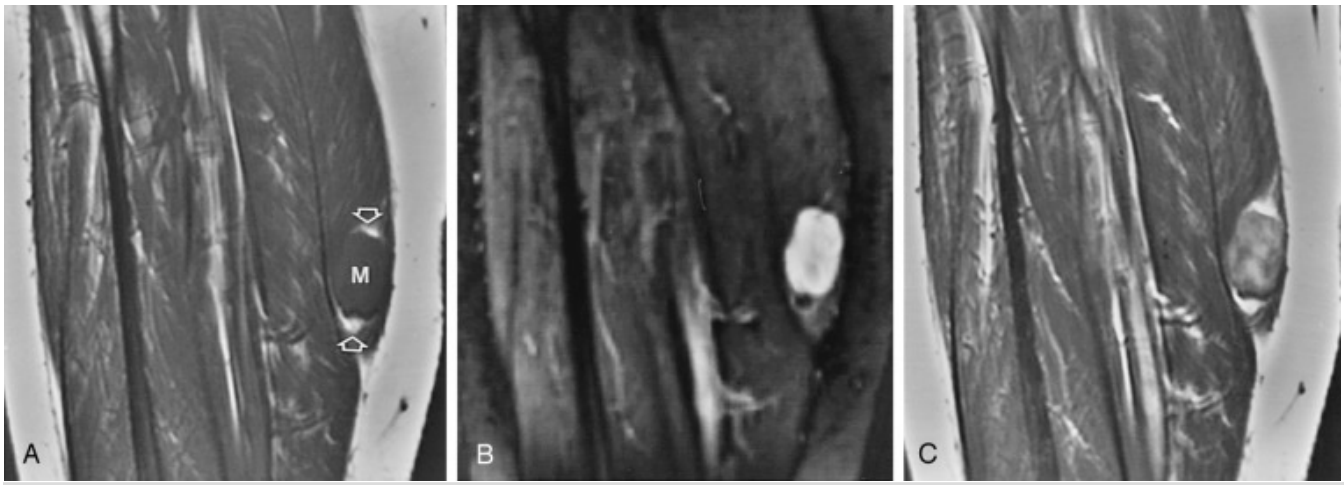

Fig. 7.38

Cystic-appearing lesion: nerve sheath tumor. **A** , T1 sagittal image. There is an ovoid, low signal intensity mass (M) within the gastrocnemius muscle (*arrows*). **B** , STIR sagittal image of the proximal calf. The mass shows mildly heterogeneous, increased signal intensity with low signal intensity centrally (target sign). **C** , T1 sagittal image of the proximal calf after administration of IV gadolinium. The mass shows heterogeneous enhancement, proving it is not a cystic lesion.

Suggested Reading

Principles of Imaging

Runge V.M.: Current technological advances in magnetic resonance with critical impact for clinical diagnosis and therapy.Invest Radiol. 2013; 48: pp. 869-877.

Bone Lesions

Kransdorf M.J., Bridges M.D.: Current developments and recent advances in musculoskeletal tumor imaging.Semin Musculoskelet Radiol. 2013; 17: pp. 145-155.

Navarro S.M., Matcuk G.R., Patel D.B., et. al.: Musculoskeletal imaging findings of hematologic malignancies.Radiographics. 2017;

37: pp. 881-900.

Zwaga T., Bovée J.V., Kroon H.M.: Osteosarcoma of the femur with skip, lymph node, and lung metastases.Radiographics. 2008; 28: pp. 277-283.

Post-therapy

Diana Afonso P., Kosinski A.S., Spritzer C.E.: Following unenhanced MRI assessment for local recurrence after surgical resection of mesenchymal soft tissue tumors, do additional gadolinium-enhanced images change reader confidence or diagnosis?.Eur J Radiol. 2013; 82: pp. 806-813.

Soft Tissue Tumors

Gruber L., Loizides A., Ostermann L., Glodny B., Plaikner M., Gruber H.: Does size reliably predict malignancy in soft tissue tumours?.Eur Radiol. 2016; 26: pp. 4640-4648.

Sammon J., Jain A., Bleakney R., Mohankumar R.: Magnetic resonance imaging appearance of soft-tissue metastases: our experience at an orthopedic oncology center.Skeletal Radiol. 2017; 46: pp. 513-521.

Sung J., Kim J.Y.: Fatty rind of intramuscular soft-tissue tumors of the extremity: is it different from the split fat sign?.Skeletal Radiol. 2017; 46: pp. 665-673.

Bone Lesion Specific

Bousson V, Rey-Jouvin C, Laredo JD, Le Merrer M, Martin-Duverneuil N, Feydy A, Aubert S, Chapurlat R, Orcel P. Fibrous dysplasia and McCune-Albright syndrome: imaging for positive and

differential diagnoses, prognosis, and follow-up guidelines. *Eur J Radiol.* 2014;83(10):1828-1842.

Campbell R.S.D., Grainger A.J., Mangham D.C., et. al.: Intraosseous lipoma: report of 35 new cases and a review of the literature.Skeletal Radiol 2003; 32: pp. 209-222.

Douis H., Parry M., Vaiyapuri S., Davies A.M.: What are the differentiating clinical and MRI-features of enchondromas from low-grade chondrosarcomas?.Eur Radiol. 2018; 28: pp. 398-409.

Gaudino S., Martucci M., Colantonio R., et. al.: A systematic approach to vertebral hemangioma.Skeletal Radiol. 2015; 44: pp. 25-36.

Keenan S., Bui-Mansfield L.T.: Musculoskeletal lesions with fluid-fluid level: a pictorial essay.J Comput Assist Tomogr. 2006; 30: pp. 517-524. Review

Malghem J., Lecouvet F., Vande Berg B.: Calcaneal cysts and lipomas: a common pathogenesis?.Skeletal Radiol. 2017; 46: pp. 1635-1642.

Mehta M., White L.M., Knapp T., et. al.: MR imaging of symptomatic osteochondromas with pathological correlation.Skeletal Radiol 1998; 27: pp. 427-433.

Murphey M.D., Kransdorf M.J.: Primary musculoskeletal lymphoma.Radiol Clin North Am. 2016; 54: pp. 785-795.

Norris M.A., Kaplan P.A., Pathria M., Greenway G.: Fibrous dysplasia: magnetic resonance imaging appearance at 1.5 Tesla.Clin Imaging 1990; 14: pp. 211-215.

O'Donnell P., Saifuddin A.: The prevalence and diagnostic significance of fluid-fluid levels in focal lesions of bone.Skeletal Radiol 2004; 33: pp. 330-336.

Wootton-Gorges S.L.: MR imaging of primary bone tumors and tumor-like conditions in children.Magn Reson Imaging Clin N Am. 2009; 17: pp. 469-487.

Soft Tissue Tumor-Lesion Specific

Bermejo A., De Bustamante T.D., Martinez A., Carrera R., Zabía E., Manjón P.: MR imaging in the evaluation of cystic-appearing soft-tissue masses of the extremities.Radiographics. 2013; 33: pp. 833-855.

Cohen J.M., Weinreb J.C., Redman H.C.: Arteriovenous malformations of the extremities: MR imaging.Radiology 1986; 158: pp. 475-479.

Crombe A., Alberti N., Stoeckle E., et. al.: Soft tissue masses with myxoid stroma: Can conventional magnetic resonance imaging differentiate benign from malignant tumors?.Eur J Radiol. 2016; 85: pp. 1875-1882.

Gaskin C.M., Helms C.A.: Lipomas, lipoma variants, and well-differentiated liposarcomas (atypical lipomas): results of MRI evaluations of 126 consecutive fatty masses.AJR Am J Roentgenol 2004; 182: pp. 733-739.

Gupta P., Potti T.A., Wuertzer S.D., Lenchik L., Pacholke D.A.: Spectrum of fat-containing soft-tissue masses at MR imaging: the common, the uncommon, the characteristic, and the sometimes confusing.Radiographics. 2016; 36: pp. 753-766.

Murphey M.D., Rhee J.H., Lewis R.B., Fanburg-Smith J.C., Flemming D.J., Walker E.A.: Pigmented villonodular synovitis: radiologic-pathologic correlation.Radiographics. 2008; 28: pp. 1493-1518.

Ng E., Tandon A.A., Ho B.C., Chong B.K.: Characterising benign fibrous soft-tissue tumours in adults: why is it so difficult and what do we need to know?.Clin Radiol. 2015; 70: pp. 684-697.

Otake S., Tsuruta Y., Yamana D., et. al.: Amyloid arthropathy of the hip joint: MR demonstration of presumed amyloid lesions in 152 patients with long-term hemodialysis.Eur Radiol 1998; 8: pp. 1352-1356.

Rubin J.I., Gomori J.M., Grossman R.I., et. al.: High-field MR imaging of extracranial hematomas.AJR Am J Roentgenol 1987; 148: pp. 813-817.

Yilmaz S., Kozakewich H.P., Alomari A.I., Fishman S.J., Mulliken J.B., Chaudry G.: Intramuscular capillary-type hemangioma: radiologic-pathologic correlation.Pediatr Radiol. 2014; 44: pp. 558-565.

References

Runge, 2013. Runge V.M.: Current technological advances in magnetic resonance with critical impact for clinical diagnosis and therapy. Invest Radiol. 2013; 48: pp. 869-877
Cross Ref (http://dx.doi.org/10.1097/01.rli.0000434380.71793.d3)

Kransdorf and Bridges, 2013. Kransdorf M.J., and Bridges M.D.: Current developments and recent advances in musculoskeletal tumor imaging. Semin Musculoskelet Radiol.

2013; 17: pp. 145-155
Cross Ref (http://dx.doi.org/10.1055/s-0033-1343070)

Navarro et al., 2017. Navarro S.M., Matcuk G.R., Patel D.B., et al: Musculoskeletal imaging findings of hematologic malignancies. Radiographics. 2017; 37: pp. 881-900
Cross Ref (http://dx.doi.org/10.1148/rg.2017160133)

Zwaga et al., 2008. Zwaga T., Bovée J.V., and Kroon H.M.: Osteosarcoma of the femur with skip, lymph node, and lung metastases. Radiographics. 2008; 28: pp. 277-283
Cross Ref (http://dx.doi.org/10.1148/rg.281075015)

Diana Afonso et al., 2013. Diana Afonso P., Kosinski A.S., and Spritzer C.E.: Following unenhanced MRI assessment for local recurrence after surgical resection of mesenchymal soft tissue tumors, do additional gadolinium-enhanced images change reader confidence or diagnosis? Eur J Radiol. 2013; 82: pp. 806-813
Cross Ref (http://dx.doi.org/10.1016/j.ejrad.2012.11.025)

Gruber et al., 2016. Gruber L., Loizides A., Ostermann L., Glodny B., Plaikner M., and Gruber H.: Does size reliably predict malignancy in soft tissue tumours? Eur Radiol. 2016; 26: pp. 4640-4648
Cross Ref (http://dx.doi.org/10.1007/s00330-016-4300-z)

Sammon et al., 2017. Sammon J., Jain A., Bleakney R., and Mohankumar R.: Magnetic resonance imaging appearance of soft-tissue metastases: our experience at an orthopedic oncology center. Skeletal Radiol. 2017; 46: pp. 513-521
Cross Ref (http://dx.doi.org/10.1007/s00256-017-2582-0)

Sung and Kim, 2017. Sung J., and Kim J.Y.: Fatty rind of intramuscular soft-tissue tumors of the extremity: is it different from the split fat sign? Skeletal Radiol. 2017; 46: pp. 665-673
Cross Ref (http://dx.doi.org/10.1007/s00256-017-2598-5)

Bousson et al., 2014. Bousson V, Rey-Jouvin C, Laredo JD, Le Merrer M, Martin-Duverneuil N, Feydy A, Aubert S, Chapurlat R, Orcel P. Fibrous dysplasia and McCune-Albright syndrome: imaging for positive and differential diagnoses, prognosis, and follow-up guidelines. Eur J Radiol. 2014;83(10):1828-1842.

Campbell et al., 2003. Campbell R.S.D., Grainger A.J., Mangham D.C., et al: Intraosseous lipoma: report of 35 new cases and a review of the literature. Skeletal Radiol 2003; 32: pp. 209-222
Cross Ref (http://dx.doi.org/10.1007/s00256-002-0616-7)

Douis et al., 2018. Douis H., Parry M., Vaiyapuri S., and Davies A.M.: What are the differentiating clinical and MRI-features of enchondromas from low-grade chondrosarcomas? Eur Radiol. 2018; 28: pp. 398-409
Cross Ref (http://dx.doi.org/10.1007/s00330-017-4947-0)

Gaudino et al., 2015. Gaudino S., Martucci M., Colantonio R., et al: A systematic approach to vertebral hemangioma. Skeletal Radiol. 2015; 44: pp. 25-36
Cross Ref (http://dx.doi.org/10.1007/s00256-014-2035-y)

Keenan and Bui-Mansfield, 2006. Keenan S., and Bui-Mansfield L.T.: Musculoskeletal lesions with fluid-fluid level: a pictorial essay. J Comput Assist Tomogr. 2006; 30: pp. 517-

Cross Ref (http://dx.doi.org/10.1097/00004728-200605000-00029)

Malghem et al., 2017. Malghem J., Lecouvet F., and Vande Berg B.: Calcaneal cysts and lipomas: a common pathogenesis? Skeletal Radiol. 2017; 46: pp. 1635-1642
Cross Ref (http://dx.doi.org/10.1007/s00256-017-2688-4)

Mehta et al., 1998. Mehta M., White L.M., Knapp T., et al: MR imaging of symptomatic osteochondromas with pathological correlation. Skeletal Radiol 1998; 27: pp. 427-433
Cross Ref (http://dx.doi.org/10.1007/s002560050412)

Murphey and Kransdorf, 2016. Murphey M.D., and Kransdorf M.J.: Primary musculoskeletal lymphoma. Radiol Clin North Am. 2016; 54: pp. 785-795
Cross Ref (http://dx.doi.org/10.1016/j.rcl.2016.03.008)

Norris et al., 1990. Norris M.A., Kaplan P.A., Pathria M., and Greenway G.: Fibrous dysplasia: magnetic resonance imaging appearance at 1.5 Tesla. Clin Imaging 1990; 14: pp. 211-215

O'Donnell and Saifuddin, 2004. O'Donnell P., and Saifuddin A.: The prevalence and diagnostic significance of fluid-fluid levels in focal lesions of bone. Skeletal Radiol 2004; 33: pp. 330-336
Cross Ref (http://dx.doi.org/10.1007/s00256-004-0779-5)

Wootton-Gorges, 2009. Wootton-Gorges S.L.: MR imaging of primary bone tumors and tumor-like conditions in children. Magn Reson Imaging Clin N Am. 2009; 17: pp. 469-487
Cross Ref (http://dx.doi.org/10.1016/j.mric.2009.03.010)

Bermejo et al., 2013. Bermejo A., De Bustamante T.D., Martinez A., Carrera R., Zabía E., and Manjón P.: MR imaging in the evaluation of cystic-appearing soft-tissue masses of the extremities. Radiographics. 2013; 33: pp. 833-855
Cross Ref (http://dx.doi.org/10.1148/rg.333115062)

Cohen et al., 1986. Cohen J.M., Weinreb J.C., and Redman H.C.: Arteriovenous malformations of the extremities: MR imaging. Radiology 1986; 158: pp. 475-479
Cross Ref (http://dx.doi.org/10.1148/radiology.158.2.3941876)

Crombe et al., 2016. Crombe A., Alberti N., Stoeckle E., et al: Soft tissue masses with myxoid stroma: Can conventional magnetic resonance imaging differentiate benign from malignant tumors? Eur J Radiol. 2016; 85: pp. 1875-1882
Cross Ref (http://dx.doi.org/10.1016/j.ejrad.2016.08.015)

Gaskin and Helms, 2004. Gaskin C.M., and Helms C.A.: Lipomas, lipoma variants, and well-differentiated liposarcomas (atypical lipomas): results of MRI evaluations of 126 consecutive fatty masses. AJR Am J Roentgenol 2004; 182: pp. 733-739
Cross Ref (http://dx.doi.org/10.2214/ajr.182.3.1820733)

Gupta et al., 2016. Gupta P., Potti T.A., Wuertzer S.D., Lenchik L., and Pacholke D.A.: Spectrum of fat-containing soft-tissue masses at MR imaging: the common, the uncommon, the characteristic, and the sometimes confusing. Radiographics. 2016; 36: pp. 753-766
Cross Ref (http://dx.doi.org/10.1148/rg.2016150133)

Murphey et al., 2008. Murphey M.D., Rhee J.H., Lewis R.B., Fanburg-Smith J.C., Flemming D.J., and Walker E.A.: Pigmented villonodular synovitis: radiologic-pathologic correlation. Radiographics. 2008; 28: pp. 1493-1518
Cross Ref (http://dx.doi.org/10.1148/rg.285085134)

Ng et al., 2015. Ng E., Tandon A.A., Ho B.C., and Chong B.K.: Characterising benign fibrous soft-tissue tumours in adults: why is it so difficult and what do we need to know? Clin Radiol. 2015; 70: pp. 684-697
Cross Ref (http://dx.doi.org/10.1016/j.crad.2015.02.010)

Otake et al., 1998. Otake S., Tsuruta Y., Yamana D., et al: Amyloid arthropathy of the hip joint: MR demonstration of presumed amyloid lesions in 152 patients with long-term hemodialysis. Eur Radiol 1998; 8: pp. 1352-1356
Cross Ref (http://dx.doi.org/10.1007/s003300050550)

Rubin et al., 1987. Rubin J.I., Gomori J.M., Grossman R.I., et al: High-field MR imaging of extracranial hematomas. AJR Am J Roentgenol 1987; 148: pp. 813-817
Cross Ref (http://dx.doi.org/10.2214/ajr.148.4.813)

Yilmaz et al., 2014. Yilmaz S., Kozakewich H.P., Alomari A.I., Fishman S.J., Mulliken J.B., and Chaudry G.: Intramuscular capillary-type hemangioma: radiologic-pathologic correlation. Pediatr Radiol. 2014; 44: pp. 558-565
Cross Ref (http://dx.doi.org/10.1007/s00247-014-2876-5)